

Master's Thesis - Integrated Climate System Sciences

Kinetics of Olivine Dissolution in Column Experiments

Aman Malik

Matriculation number: 1234567

Born: 15 October 1990 in Nice City, Country

School of Integrated Climate System Sciences

University of Hamburg

Hamburg, 26.01.2017

This thesis has been accepted as a Master Thesis by the Department Geowissenschaften der Universität Hamburg.

First Supervisor: Prof. Dr. Jens Hartmann, Institute of Geology, University of Hamburg

Second Supervisor: Dr. Thorben Amann, Institute of Geology, University of Hamburg

This is a contribution to the title: Kinetics and mechanism of olivine dissolution in column experiments

Abstract

The application of powdered silicate rock on land to absorb CO₂ requires knowledge of the rate of the reaction and factors affecting it. Rate measured using mixed-flow reactors and batch reactors may be inaccurate for this purpose because of the low rock to volume ratio, pre-treatment of grains, and short run time. This work fulfills the gap by conducting batch-type column experiments with olivine over a long time (~1 y). The results indicate the system has yet to achieve steady-state. The coarse grain-type have higher rate than fine-type and rates differ depending on the reaction product; these are several orders of magnitude smaller than past experiments. Surface-limited rate control or experimental errors cannot explain these results. A theoretical rate model for a packed bed of forsterite is used taking variables from the experiment. The similarity of model and experimental results indicate that the system is predominantly transport-controlled. The results might be relevant in understanding results from column experiments in general and the discrepancy between field and laboratory weathering rates.

Contents

List of Figures	v
List of Tables	vii
Abbreviations	viii
1 Introduction	1
1.1 Weathering of rocks	1
1.2 Structure of the thesis	2
2 Background and Literature Review	3
2.1 Forsterite	3
2.2 Enhanced Weathering	3
2.3 Calculating the reaction rate	5
2.4 Reaction control in mineral dissolution	6
2.4.1 Transport and Surface processes	7
2.5 Characteristics of Forsterite dissolution	7
2.5.1 Nonstoichiometry	7
2.5.2 Non steady state	8
2.5.3 Factors affecting rate of dissolution	8
2.5.4 Rate control in forsterite dissolution	11
2.6 Motivation	12
3 Materials and Methods	13
3.1 Olivine characterisation	13
3.2 Experimental setup	15
3.3 Solution analysis	15

4	Results and Discussion	18
4.1	Major ion analysis	18
4.2	Thickness of ‘surface layer’	22
4.3	Pore volume and Residence time	22
4.4	Rate of Reaction	26
4.4.1	Rate comparison with literature	28
4.4.2	Transport control in column reactors	31
5	Conclusions, Implications, and Future Work	34
6	Appendix	36
6.1	Climate Engineering and CDR options	36
6.2	Enhanced Weathering and Mineral Carbonation	37
6.3	Molecular formula of olivine	38
6.4	BET analyses	38
6.5	Calculation of thickness of the ‘surface layer’	40
6.6	Minor ion analysis	43
	Bibliography	46
	Acknowledgments	51

List of Figures

2.1	Atomic structure of forsterite with unit cell (marked in black). Oxygen is shown in red, silicon in pink, and Mg in blue.	4
2.2	Factors affecting rate control in silicate dissolution. The double sided arrows represent the possibility when both processes become important or influence each other. The surface processes are taken for forsterite but the transport processes are generic.	11
3.1	Particle size distribution of fine (a) and coarse (b) grain-type particles. The fractional weight (%) is the fraction of olivine retained on a sieve of a particular aperture size (expressed as mean particle diameter here). Results prepared by colleagues in the working group Sedimentology and Stratigraphy at the University of Hamburg	14
3.2	Scanning electron microscope (SEM) image of an olivine grain showing a coarse particles and the many fines and ultrafines adhering to it (Keitzel, 2015).	14
3.3	Illustration of the column design	16
3.4	Experimental setup showing arrangement of the columns containing olivine (1 to 3 are coarse, 4 to 6 are fine, and 7 to 9 are mixed), rhizones to collect pore water, and containers to collect outlet water.	16
4.1	The outlet $[Mg^{+2}]$ plotted against the Time (Date), averaged for the three grain types- fine, coarse, and mixed.	19
4.2	The outlet Alkalinity plotted against Time (Date), averaged for the three grain types- fine, coarse, and mixed.	20
4.3	The outlet Dissolved Silica (DSi) plotted against Time (Date), averaged for the three grain types- fine, coarse, and mixed.	21
4.4	The ratio of Mg/Si plotted against time and averaged for the three grain-types — fine, coarse, and mixed.	22

4.5	Flow rate (cm^3s^{-1}) vs. Time (Date). The results are averaged for the three grain types- fine, coarse, and mixed. The black line is the linear fit. R^2 is the regression coefficient.	24
4.6	Residence Time (days) plotted with the progress of the reaction (Date), for the three grain types— fine, coarse, and mixed. The black line is a linear fit and shows the general trend. R^2 is the regression coefficient.	25
4.7	The rate of reaction in terms of Mg, Alkalinity, and DSi (in $\text{mol m}^{-2}\text{s}^{-1}$) plotted against Time (Date), averaged for the three grain types— fine, coarse and grain and over week.	27
4.8	Rate data (in terms of $\log r_{\text{BET}} \text{Mg}^{+2}$) vs. pH from past experiments on forsterite dissolution (Rimstidt et al., 2012). The black line is the pH of interest. The range of Mg, Alkalinity, Si rates shown in orange, green, and red respectively.	29
4.9	pH of the outlet water plotted against Time (Date) for the three grain types — fine, coarse, and mixed.	30
4.10	Plot of Log Rate of dissolution (in $\text{mol m}^{-2}\text{s}$), vs. Temperature ($^{\circ}\text{C}$) at pH 8. The purple curve is the reaction flux (J_R) and is the same for fine and coarse grain types. J_D is the dissolution flux for fine (green) and coarse (blue). The green and red bar are the range of measured values for Mg and Si respectively. The grey band is the temperature range of interest.	33
6.1	Schematic illustration of CE technologies. Source: kiel-earth-institute - own work, https://commons.wikimedia.org/w/index.php?curid=38682676	36
6.2	Plot of SSA ($\text{m}^2 \text{g}^{-1}$) measured by BET vs. particle diameter (μm) obtained through past studies.	40
6.3	Plot of cumulative contribution of a particle with diameter D to the total of the surface areas (in percent) vs. mean particle diameter (in μm) for fine grain-type	41
6.4	The concentration of minor ions - Ca^{+2} , K^{+} , and Na^{+} with time (Date), averaged over the three grain types - fine, coarse, and mixed.	44
6.5	The concentration of minor ions - NO_3^{-} , Cl^{-} , and SO_4^{2-} with time (Date), averaged over the three grain types - fine, coarse, and mixed.	45

List of Tables

2.1	Lifetime of a hypothetical 1 mm sphere in a solution at pH 5, in years, for different minerals (Lasaga, 1995). The minerals listed are various silicates and a few carbonates.	5
3.1	Specific surface area measured using BET for the two grain types.	13
3.2	Mineral composition from XRF analysis (Keitzel, 2015)	16
3.3	Physical characterisation of olivine in the columns with column number, grain-type, weight and total surface area (TSA)	17
4.1	Table showing the pore volume and porosity for different columns.	23
4.2	Variables pertaining to the current experiment entered into the model of Rimstidt (2015)	32
6.1	Summary of main differences between Enhanced weathering and Mineral carbonation	37
6.2	BET measured specific surface area for the two grain types- fine and coarse.	39
6.3	Comparison of measured and estimated SSA ($\text{m}^2 \text{g}^{-1}$)	40
6.4	Mean diameter and weight fraction from laser granulometry, SSA from regression equation, and surface area as the product of weight fraction and BET area for fine grain-type.	42
6.5	Mean diameter and weight fraction from laser granulometry, SSA from regression equation, and surface area as the product of weight fraction and BET area for coarse grain-type.	43
6.6	Results for Mg and Si released, observed, and precipitated. The Si precipitated converted to thickness of layer.	44

Abbreviations

BET Brunauer-Emmett-Teller

BR Batch Reactor

CDR Carbon dioxide Removal

CE Climate Engineering

DSi Dissolved Silica

EW Enhanced Weathering

MFR Mixed Flow Reactor

PFR Plug Flow Reactor

RT Residence Time

TSA Total Surface Area

XRF X-ray Fluorescence

Chapter 1

Introduction

1.1 Weathering of rocks

Rocks formed deep inside the earth, when exposed on or near to the surface, adapt or re-equilibrate to their new surroundings by disintegration and decomposition through chemical and physical forces of the atmosphere, hydrosphere, and biosphere. This process is known as weathering ([Manutchehr-Danai, 2009](#)). The chemical weathering of rocks releases elements into the environment which may be absorbed by plants, deposited and sequestered in soils and other rocks, or end up in the oceans ([Hellmann et al., 2012](#)). One family of minerals in particular, those belonging to Ca- and Mg- silicates¹, are known for their fast weathering rates and have influenced CO₂ concentrations in the atmosphere over 10⁵–10⁶ y timescales, thereby impacting the global carbon cycle ([Brantley, 2008a](#)). That, in turn, has influenced the global climate through feedback processes ([Renforth et al., 2015](#)). Thus, quantifying silicate weathering rates and the associated global atmospheric CO₂ concentration has been the focus of many past studies ([Golubev et al., 2005](#)). The current interest in silicate dissolution rates stems from its application in CO₂ removal techniques like enhanced weathering.

The rates of silicate dissolution and factors controlling the rate have been studied through laboratory experiments for over half a century. However, the same methods when applied in the field have consistently produced much lower rates than observed in laboratory conditions ([White and Brantley, 1995](#)). Factors explaining this divergent behaviour have not been successfully quantified ([Renforth et al., 2015](#)). The question remains if laboratory results are good enough to produce desirable results for enhanced weathering application at field scale. The current thesis attempts to answer this question by undertaking long-term

¹A group of silicon-oxygen compounds

laboratory experiments closely mimicking the proposed application.

1.2 Structure of the thesis

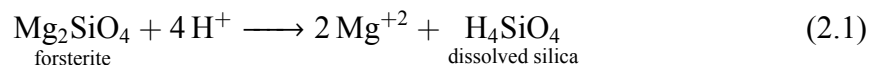
Chapter 2, Background and Literature Review, summarises the concepts and terminologies associated with rate of mineral dissolution and factors influencing it; followed by the motivation for the current work. Chapter 3, Materials and Methods, describes the laboratory setup and the instruments used to analyse physical and chemical properties of the mineral and water samples. Chapter 4, Results and Discussion, consists of results of the experiment, importantly the reaction rate, and discusses the variables affecting it. Chapter 5, Conclusions, summarises the findings in the light of past work and its implication to weathering research and enhanced weathering application. Additional information and calculations are presented in the Appendices.

Chapter 2

Background and Literature Review

2.1 Forsterite

The Olivine group of silicate minerals typically contain two end-members: Forsterite, a Mg-silicate, and Faylite, an Fe-silicate, and are abbreviated as Fo and Fa respectively. Naturally occurring olivine is richer in forsterite ([Johnson et al., 2004](#)) in [Bearat et al. \(2006\)](#), for e.g., dunite contains at least Fo_{92} (92 % forsterite and 8 % fayalite by mole) and peridotite typically $\geq Fo_{88}$. The dissolution reaction of forsterite in a closed system follows the reaction:



Among the many natural occurring silicates, forsterite is an example of a neosilicate. In neosilicates, the silica (SiO_4) tetrahedra is unpolymerized, i.e., it does not share any oxygen molecules with other silicate tetrahedrons, but instead balances its charge through ionic bonds with interstitial cations like Mg^{+2} ([Tilley and Simmons, 2016](#)). This absence of strong interconnecting Si – O – Si bonds makes it the fastest weathering silicate mineral. The structure of forsterite is illustrated in [Figure 2.1](#).

2.2 Enhanced Weathering

Enhanced weathering (EW) is one of many carbon dioxide removal (CDR) technologies under the umbrella of climate engineering¹. It aims to accelerate the natural process of weathering by application of powdered minerals over land, ocean, or coastal zones (([Schuiling](#)

¹For more information on climate engineering and CDR see section [6.1](#)

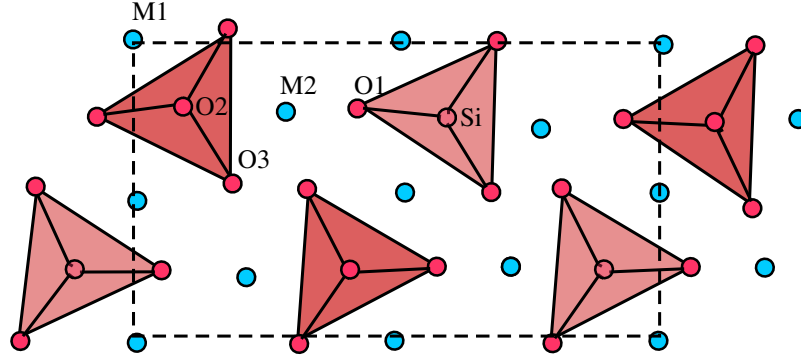
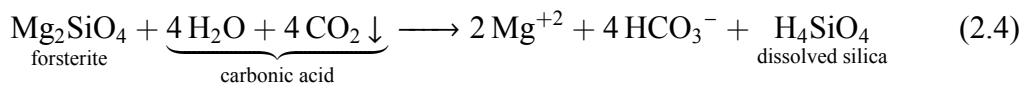
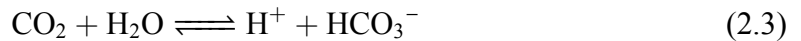
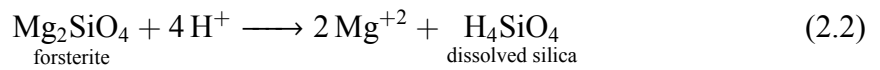


Figure 2.1: Atomic structure of forsterite with unit cell (marked in black). Oxygen is shown in red, silicon in pink, and Mg in blue.

and Krijgsman, 2006; Hangx and Spiers, 2009) in Renforth et al. (2015)). The land application is suitable in warm and humid tropical areas on soil with low pH (Schuiling and Krijgsman, 2006; Köhler et al., 2010). The suitability of a rock or mineral for EW depends, among other variables, on its reactivity and abundance. Forsterite (Mg-olivine) has one of the highest dissolution rates found in nature² (See Table 2.1). Furthermore, rocks like peridotite, basalt, gabbro, and dunite contain the highest concentration of fast weathering silicates, like olivine (Hartmann et al., 2013), and constitute around 15 % of the total land surface area (Meybeck, 1987; Hartmann and Moosdorf, 2012). These factors make forsterite a preferred choice for EW application.

The absorption of CO₂ from the atmosphere in a silicate dissolution reaction is a combination of two reactions. The first reaction is of forsterite with a proton (H⁺), shown in Equation (2.2). The second is the equilibrium reaction of CO₂ and water (see Equation (2.3)). As H⁺ is consumed in reaction 2.2, the equilibrium reaction 2.3 counteracts this disturbance by absorbing more CO₂ (Le Chatelier's principle) thereby producing more H⁺ and HCO₃⁻. These two reactions are written as a single reaction in Equation (2.4). Stoichiometrically, 4 mol of CO₂ are absorbed for every 1 mol of forsterite reacted. In terms of mass, 1 g of forsterite absorbs ~1.25 g of CO₂.



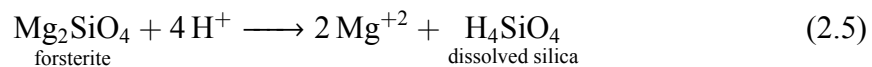
²Carbonates have very high dissolution rates but could be limited in their application due to the high saturation state of dissolved carbonates in oceans. When supersaturated, the 'extra' calcium and carbonate ions would precipitate to produce carbonate and release CO₂ back into the atmosphere.

Mineral	Dissolution Time (years)
Quartz	34,000,000
Kaolinite	6,000,000
Muscovite	2,600,000
Epidote	923,000
Microline	921,000
Biotite	900,000
Albite	575,000
Andesine	80,000
Bytownite	40,000
Enstatite	10,100
Diopside	6,800
Forsterite	2,300
Dolomite	1.6
Calcite	0.1

Table 2.1: Lifetime of a hypothetical 1 mm sphere in a solution at pH 5, in years, for different minerals (Lasaga, 1995). The minerals listed are various silicates and a few carbonates.

2.3 Calculating the reaction rate

The reaction rate is defined as the rate of change of concentration of reactants or products. For the dissolution of forsterite (Equation (2.5)), this rate is expressed as Equation (2.6). r is the extent of reaction and n_{fo} are the moles of forsterite. Further, reactions occurring at the mineral/fluid boundary, also called heterogeneous reactions, are often shown to be dependent on the total or reactive surface area. Hence, the comparison of mineral reaction rates is often done based on rates normalised to surface area ($\text{mol m}^{-2} \text{s}^{-1}$).



$$r = -\frac{dn_{fo}}{dt} = -\frac{1}{4} \frac{d[\text{H}^+]}{dt} = \frac{1}{2} \frac{d[\text{Mg}]^{+2}}{dt} = \frac{d[\text{H}_4\text{SiO}_4]}{dt} \quad (2.6)$$

The rates of chemical reactions, as a function of time or species concentration, are measured in chemical reactors (Brantley, 2008b). A batch reactor (BR) consists of a tank which is continuously stirred to maintain a homogeneous concentration. As the reaction proceeds small samples, called aliquots, of the solution are removed to observe the change

in concentration of product, say $[Z]$. The reaction rate is calculated as follows:

$$r = \frac{1}{A_s m} \frac{dn_Z}{dt} \quad (2.7)$$

where n_Z is moles of element Z in solution, t is time in seconds, A_s is the surface area of mineral in m^2 , m is the mass of the mineral in grams. In Equation (2.7), it is assumed that the aliquots are so small that it doesn't influence the total volume of the reactor.

Continuously stirred reactor (CSTR) also called mixed flow reactor (MFR) are flow-through reactors where a mineral is placed in a vessel through which fluid is continuously pumped at flow rate Q (Brantley, 2008b). Unlike BR where the the reactor volume can change as aliquots are drawn out over long run, MFR continuously pump liquid in and out of the vessel, such that the volume remains constant. The minerals are suspended in the vessel to maintain ideal mixing. The rate is calculated as:

$$r = \frac{Q([Z_o] - [Z_i])}{A_s m} \quad (2.8)$$

where Q is the flow rate, $[Z_o]$ and $[Z_i]$ are the outlet and inlet concentrations respectively, A_s and m are as before.

A Plug-flow reactor (PFR), also referred as column reactors (when run vertically) or packed-bed reactors are more complex than BR or MFR because of non-ideality of flow and precipitation of products (Brantley, 2008b). When the inlet rate is the same as the outflow rate, the rate is calculated as (White and Brantley, 2003):

$$r = \frac{Z_o - Z_i}{\beta A_s} \frac{dV}{dt} \quad (2.9)$$

where Z_i and Z_o are inlet and outlet concentrations respectively, β is the stoichiometric coefficient, A is the mineral surface area, and dV/dt is the rate of flow of fluid through the reactor. Thus, the rate is directly proportional to the product of the (outlet- inlet) concentration and flow rate, and inversely proportional to the surface area.

2.4 Reaction control in mineral dissolution

In any chemical reaction with multiple steps, the rate of the slowest reaction governs the overall rate of the reaction. The dissolution of minerals occurs through the combination of two distinct processes: the transport of aqueous reactants and products - to and from the surface, and the chemical reactions occurring at the surface (Schott et al., 2009). These

processes can occur with similar or different rates. If transport of reactants to the surface is faster than the reactions at the surface, the reaction is **interface/surface- controlled**, or **transport-controlled** when vice-versa. When their rates are comparable, both processes become important. The terms ‘controlled’ and ‘limited’ have been interchangeably used in the text.

2.4.1 Transport and Surface processes

Transport processes can broadly be divided into advection and diffusion. Advection carries away reaction products and transports reactive species from distant regions to the vicinity of the reacting mineral (Rimstidt, 2015). Advection of a fluid occurs through mechanical agitation, like in a MFR, or when the fluid is subjected to a pressure difference (Rimstidt, 2013). The latter can also happen due to nonuniform distribution of salinity and temperature. Diffusion, on the other hand, is driven by concentration gradients across — a fluid boundary layer (the thin layer of immobile fluid in contact with the mineral surface) (Rimstidt, 2015), an alteration layer/leached layer on the mineral surface (Luce et al., 1972; Brantley, 2008a), solid-state diffusion (Luce et al., 1972), or a combination of the three. The transport rate is measured as a transport flux with units of $\text{mol m}^{-2} \text{s}^{-1}$.

Surface processes refer to the basic molecular steps leading to detachment of a cation or other atom from the mineral bulk into the bulk solution (Luttge and Arvidson, 2008). These processes depend on the physical and chemical properties of the mineral (also called intrinsic factors) (White, 2002), for e.g., molecular composition, reactive surface area etc.; they are discussed in detail in Section 2.5.

2.5 Characteristics of Forsterite dissolution

2.5.1 Nonstoichiometry

A reaction is stoichiometric and shows congruent dissolution when the consumption of reactants and release of products follow the reaction stoichiometry. For equation (2.5), this would mean that 1 mol of forsterite dissolves completely to produce 2 moles of Mg^{+2} and 1 mol of dissolved silica (H_4SiO_4). However, many silicates show nonstoichiometry and thus incongruent dissolution. This behaviour can be due to dissolution of impurities within the mineral, by precipitation of secondary minerals, or by preferential leaching of elements from the mineral surface (Brantley, 2008a). Past experiments on forsterite dissolution have observed nonstoichiometry in the initial phase of the dissolution (becoming stoichiometric

after a few hundred hours of reaction); that has been attributed to the formation of a Si-rich amorphous layer on the mineral surface (Wogelius and Walther, 1992; Pokrovsky and Schott, 2000; Hellmann et al., 2012). Nonstoichiometry is more pronounced at lower pH. At steady state, the thickness of this layer has been reported to be around 1–5 nm (Pokrovsky and Schott, 2000; Hellmann et al., 2012) at 25 °C.

Until recently, the formation of the Si-rich layer was believed to be due to the preferential leaching of Mg compared to Si (Luce et al., 1972; Paces, 1973; Pokrovsky and Schott, 2000; Lee et al., 2008) followed by the slow hydrolysis and subsequent leaching/release of the Si and O into the bulk solution. This resulted in the formation of an outer layer, rich in Si or depleted in Mg, called leached or depleted layer after the mechanism involved. Hellmann et al. (2012), however, using high-resolution images showed that both Mg and Si dissolve congruently into the solution irrespective of the pH and involve no preferential leaching. Only Si reprecipitates back on the surface leading to formation of the Si-rich layer. This theory of dissolution-reprecipitation calls the Si-rich layer simply as a surface layer. The mechanism and terminology from Hellmann et al. (2012) will be used in the text.

2.5.2 Non steady state

The first experiments on forsterite dissolution in mixed-flow reactors observed the reaction rate to decrease with time as a power function of the form $r = kt^{0.5}$ (Luce et al., 1972; Paces, 1973), giving rise to the term *parabolic kinetics* (Brantley, 2008a). This non-steady state behavior is attributed to the initial fast dissolution of fine particles and surface sites with high energy (created during the crushing and grinding of a mineral), as well as non-stoichiometric dissolution (Holdren and Berner (1979) in Brantley (2008a)). However, cleaning of the initial material to remove fines and using a low rock to fluid volume ratio result in apparent steady state rates in a few hundred hours and thus provide a means of comparison across experiments.

2.5.3 Factors affecting rate of dissolution

The following section summarises the most up-to-date knowledge on factors affecting rate of forsterite dissolution, particularly at ambient temperatures and above neutral to alkaline pH range, and the conceptual or experimental problems associated with their measurement.

Effect of pH and temperature

The effect of pH and temperature on rate of forsterite dissolution has been rigorously studied (Wogelius and Walther, 1991, 1992; Pokrovsky and Schott, 2000; Rosso and Rimstidt, 2000; Oelkers, 2001). The effect of the main factors on the rate has been summarised by Rimstidt et al. (2012) into a rate equation (normalised to BET surface area):

$$\log \text{Rate}_{\text{BET}} = 5.17 - 0.44\text{pH} - 3675/T \quad \text{for pH} < 5.6 \quad (2.10a)$$

$$\log \text{Rate}_{\text{BET}} = 2.34 - 0.22\text{pH} - 3179/T \quad \text{for pH} > 5.6 \quad (2.10b)$$

Equation (2.10) show that the reaction rate is directly proportional to the pH, or $[\text{H}^+]$, and the Temperature.

Effect of particle size and surface area

Along with temperature and pH, the surface area is the most important factor controlling reaction rate (Rimstidt et al., 2012). However, unlike pH and temperature, it has not been rigorously studied for forsterite.

Comparison of reaction rates (at similar conditions) from past studies reveals large errors (~ 0.5 log units) when normalised to geometric surface area (Rimstidt et al., 2012). These errors were attributed to experimental and conceptual problems. The experimental problems concern with factors affecting BET measurement— preparation of sample, pre-treatment of sample, mineral composition and adsorbent gas used (Brantley and Mellott, 2000; Rimstidt et al., 2012; Rosso and Rimstidt, 2000). Even though BET measurements of a same sample on the same machine are highly reproducible (error of $\pm 5\%$ (Brantley and Mellott, 2000)), the factors mentioned above become important when measurements are compared across laboratories.

A mineral surface is composed of sites with different surface energies and the reactivity of a mineral is controlled by the number and distribution of these sites, and the crystallographic axes (Grandstaff, 1978; Awad et al., 2000; Luttge and Arvidson, 2008). These constitute the reactive (White and Peterson, 1990) or the effective surface area (Aagaard and Helgeson, 1982; Helgeson et al., 1984). However, most studies on finding dissolution rates don't use them; instead, the total surface area (TSA) (also known as the BET surface area), or the geometric surface area is used (Luttge and Arvidson, 2008). This assumption implies that reacting sites are homogeneously distributed and all surface sites are equally reactive (Grandstaff, 1978; White and Peterson, 1990). Moreover, the relation between surface area and reaction rate is assumed to be the same across all grain sizes (Grandstaff,

1978). Holdren and Speyer (1987) experimenting with feldspars, show that this assumption breaks down for particles $<75\text{ }\mu\text{m}$ and that for particles in this region no clear relation exists between rate and surface area. This result is also supported by experiments of Kleiv and Thornhill (2006).

Lastly, reaction rates are often normalised to initial surface area (geometric or BET) but the reaction at any moment depends on the reactive surface area available at a particular point of time.

The above mentioned points highlight the experimental problems and conceptual assumptions associated with surface area. These must be considered on any discussion or comparison of reaction rates.

Effect of reaction products and other ions

The effect of reaction products (see equation (2.1)) on reaction rate have been explored by a few studies. Oelkers (2001) observe that forsterite dissolution rates are unaffected by aqueous Mg and Si at pH 2, whereas Pokrovsky and Schott (2000) show that the rate decreases at pH 9 and 11 as a function of Si concentration. Both experiments were carried in MFRs at 25 °C. Rimstidt et al. (2012) summarise that water activity (>0.9), $[\text{SO}_4^{2-}] > 3\text{ M}$, and Ionic Strength $<12\text{ M}$ do not significantly affect rates.

Effect of CO_2 and carbonates

Even though most laboratory experiments on forsterite dissolution were held in closed systems and took into account only hydrolysis of forsterite, real world application — for calculating natural CO_2 consumption through weathering, enhanced weathering, or mineral carbonation require the interaction of the basic hydrolysis reaction with CO_2 or dissolved carbonate ions. These could influence rate directly - by formation of surface complexes during interaction, or indirectly - by control of pH (Awad et al., 2000). The overall effect of dissolved CO_2 on forsterite dissolution isn't understood because of contradictory results. Golubev et al. (2005) reported that there is no effect of $p\text{CO}_2$ (p is partial pressure) on the rate of dissolution, while Wogelius and Walther (1991) reported a decrease in the rate of dissolution of olivine. Further, the effect of $p\text{CO}_2$ might be dependent on the pH and that it might be important in alkaline conditions (Hänchen et al., 2006; Wogelius and Walther, 1991). According to Rimstidt et al. (2012) existing data set is not sufficient to quantify any affect of dissolved carbonates, and even under alkaline conditions at constant pH, silicate dissolution rates show only a negligible or at best weak dependence on $p\text{CO}_2$ (Luttge and Arvidson, 2008).

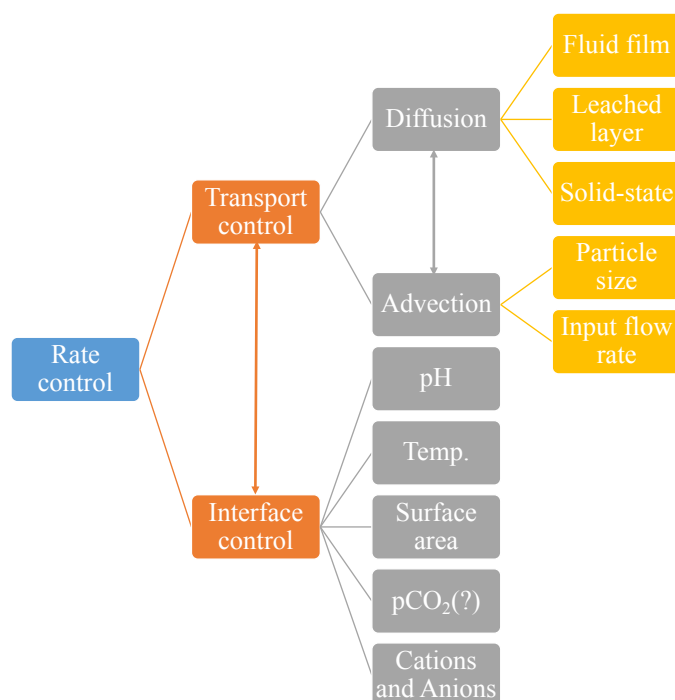


Figure 2.2: Factors affecting rate control in silicate dissolution. The double sided arrows represent the possibility when both processes become important or influence each other. The surface processes are taken for forsterite but the transport processes are generic.

2.5.4 Rate control in forsterite dissolution

Results from previous studies point toward the dissolution of forsterite being surface limited. According to [Schott et al. \(2009\)](#), for most rock-forming minerals³ at ambient temperatures, chemical reactions at the solid interface are slow and thus rate limiting. [Wogelius and Walther \(1991\)](#); [Brady and Walther \(1989\)](#) show that the control of dissolution reactions for silicates clearly occurs at the surface. To test for transport control in laboratory experiments [Luce et al. \(1972\)](#) changed the agitator speed of the reactor but found no change in the reaction rate, implying surface control. The concept of reaction control can also be understood in terms of energy requirements — at low temperatures the activation energy of the of the mineral interface (~ 15 kcal/mol) is often higher than that of diffusion (~ 5 kcal/mol) ([Brantley, 2008a](#)). Perhaps for the same reasons mentioned above, [Rimstidt et al. \(2012\)](#), in their compilation of past studies assume rate to be interface limited for all experiments even though there was insufficient information in the literature to quantify the hydrodynamics ([Rimstidt et al., 2012](#)). However, most laboratory experiments on forsterite dissolution have been carried out at small rock to volume ratios, i.e., a few grams or milligrams of

³Forsterite is also a rock-forming mineral

the mineral are taken in comparatively large batch and mixed-flow reactors (Awad et al., 2000; Martinez et al., 2014) and thus might not have been susceptible to transport control. Among various reactor designs, Plug-Flow Reactors (PFRs) with packed-beds (also called packed-bed reactors) are highly susceptible to be transport-controlled and also better mimic natural systems (Brantley, 2008b), but few experiments with packed beds exist for forsterite. For e.g., in the compilation of past forsterite dissolution studies (Rimstidt et al., 2012) only one experiment, that of Kleiv and Thornhill (2006), was performed in a PFR. More recently, Renforth et al. (2015), conducted packed-bed experiments on a mixture of olivine and soil. An illustrative flow-chart on the factors affecting rate-control in forsterite is shown in Section 2.5.3.

As discussed in section 2.4.1, the diffusion of reactants or products between the bulk-solution and the mineral surface occurs across a layer/region. This layer could be the immobile fluid boundary layer, leached/altered layer, or the solid itself. Hellmann et al. (2012) argue that both the Si-rich layer formed on forsterite or solid-state diffusion are not rate controlling, mainly because of the small thickness and high porosity of the altered layer. Rimstidt (2015) through modeling studies for a packed bed/column of forsterite and assuming diffusion of H^+ through a fluid film show that under certain conditions rate can become transport-limited. This model will be used and discussed in detail later.

2.6 Motivation

The application of olivine or other silicate containing rock for EW can be imagined as spreading of rock powder on, for e.g., agricultural farms resulting in a layer/column of the material. The current study aims to find the kinetics of olivine dissolution in column experiments and to understand the variables affecting it.

Chapter 3

Materials and Methods

3.1 Olivine characterisation

Olivine, available as Oliflux™, was obtained from Devo bouwstoffen b.v, a Dutch company. The likely source of the rock is the peroditite quarry in Åheim, Norway. The olivine was supplied in two grades — labelled as containing predominantly grain size fractions of $<63\text{ }\mu\text{m}$ and $0\text{--}3\text{ mm}$ which we call *fine* and *coarse* respectively. The specific surface area of the grain types was analysed using the multi-point BET method in a Quantachrome autosorb iQ™ surface area analyser, using N_2 as the adsorbant gas. The results are listed in Table 3.1 (see section 6.4 for details on the BET method). The particle size distribution was obtained using laser granulometry. The spread is across 2 orders of magnitude for both, coarse ($\sim 1\text{ }\mu\text{m}$ to $\sim 2\text{ mm}$), and fine ($\sim 0.15\text{--}100\text{ }\mu\text{m}$) (see Figures 3.1a and 3.1b). Especially of interest are the percentages of ultrafines ($<10\text{ }\mu\text{m}$), because of their large specific surface area contribution (see Section 6.4 for calculations). The presence of these ultrafine particles can also be seen in the scanning electron microscope (SEM) images (Figure 3.2).

The chemical analysis of the olivine was performed using X-ray fluorescence spectroscopy (XRF) (Table 3.2). The molecular formula of the olivine is determined as $\text{Mg}_{1.88}\text{Fe}_{0.12}\text{SiO}_4$ (see Section 6.3 for calculations).

Grain type	Specific surface area ($\text{m}^2\text{ g}^{-1}$)
$<63\text{ }\mu\text{m}$, fine	9.53 ± 0.43
$0\text{--}3\text{ mm}$, coarse	1.06 ± 0.10

Table 3.1: Specific surface area measured using BET for the two grain types.

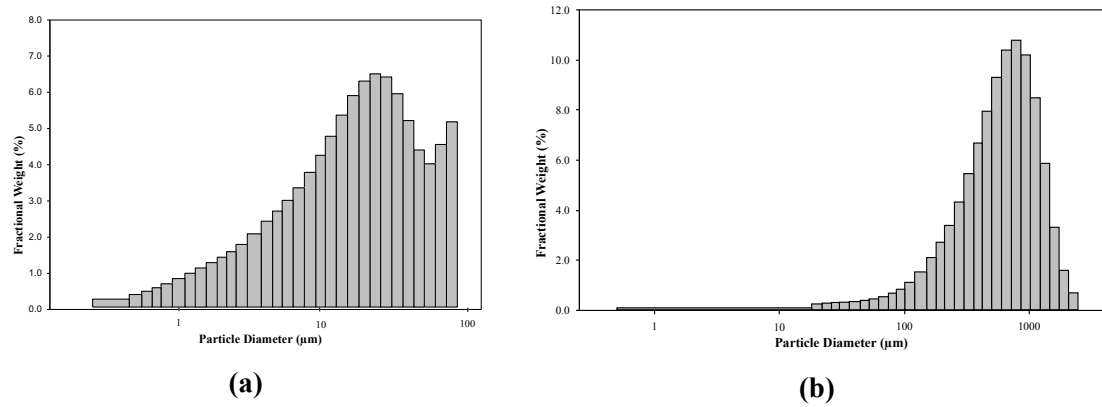


Figure 3.1: Particle size distribution of fine (a) and coarse (b) grain-type particles. The fractional weight (%) is the fraction of olivine retained on a sieve of a particular aperture size (expressed as mean particle diameter here). Results prepared by colleagues in the working group Sedimentology and Stratigraphy at the University of Hamburg

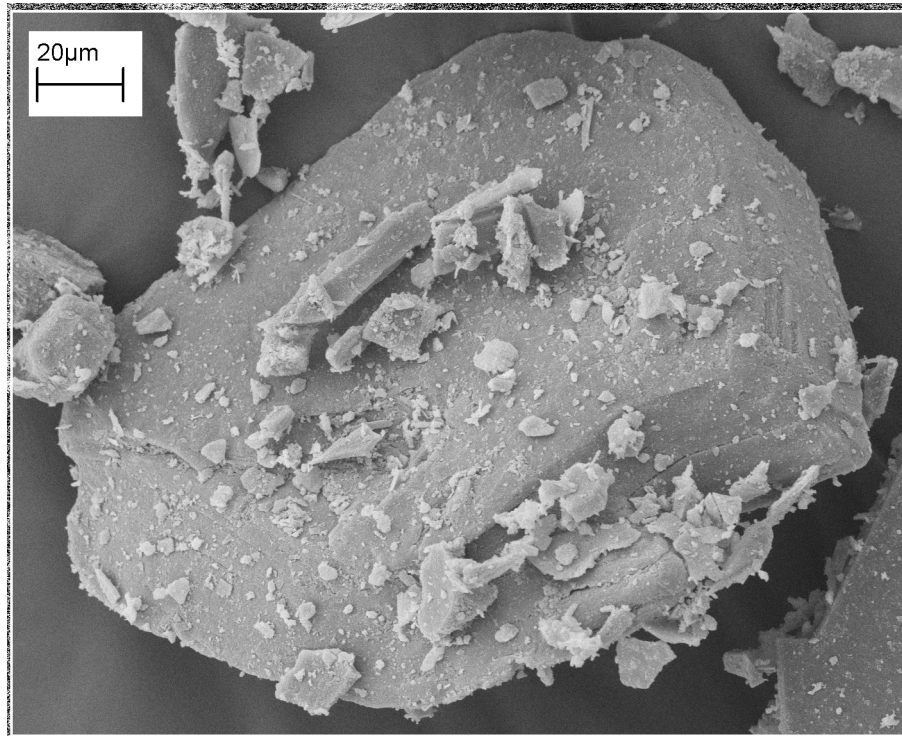


Figure 3.2: Scanning electron microscope (SEM) image of an olivine grain showing a coarse particles and the many fines and ultrafines adhering to it (Keitzel, 2015).

3.2 Experimental setup

The setup (see Section 3.2 and figure 3.4) consisted of nine acrylic cylindrical tubes with outer diameter/inner diameter/height of 60/56/250 mm respectively. A 20 μm nylon mesh¹ was fixed at the bottom of each cylinder using electrical tape. The nylon mesh allowed water to flow through but not the rock powder. Three holes were drilled at 5 cm intervals (measured from bottom) for each cylinder, to allow insertion of Rhizons. A Rhizon² is a micro-filtering membrane used to extract pore water samples from soil layers or sediments. Crushed olivine without any chemical pre-treatment was filled till 20 cm height (measured from bottom), tapping the cylinder along the way to compress the powder. The first three cylinders contained coarse grain-type (0–3 mm), the next three fine grain-type (<63 μm) and the last three were a 1:1 mixture by weight of the two grain types. The weight of the olivine powder in each cylinder was subsequently measured. The total surface area (TSA) was calculated by multiplying the weight of the olvine in each column to the specific surface area measured by BET. The results are listed in Table 3.3. All cylinders stood upright using clamps and clamp-stands. The opening was covered with aluminum foil to decrease water loss by evaporation. Outlet/exit water was collected in plastic bottles. The setup was kept in an air-conditioned room set at 25 °C but room thermometers showed variation between 22–26 °C during the duration of the experiment.

The experiment started on 5 June 2015 and continues to date although data is analysed only till 14 March 2016. 75 ml of ultrapure Milli-Q™ (conductivity of 18 M Ω) was added to each cylinder, five days a week. Thus, the total amount of water added (excl. weekends and holidays) was (274×74) 20.55 l. The sampling frequency, i.e., how often water samples are collected from the outlets and rhizons changed during the experiment run. During the first four months, outlet samples were collected every day while rhizon samples were collected twice a week. The frequency was subsequently decreased, to bimonthly for both outlet and rhizons, and currently only monthly measurements are taken.

3.3 Solution analysis

The outlet samples were measured for pH, total alkalinity, dissolved silica, and major ion composition. Total alkalinity was measured using a Metrohm Titrand 818™ up to a pH endpoint of 4.3. The Si concentration is measured as dissolved silica $\text{Si}(\text{OH})_4$ and measured using the molybdate blue colometric method. The major ion composition was determined

¹Hydro-Bios, <http://www.hydrobios.de/plankton-nets/>

²Rhizosphere, <http://www.rhizosphere.com/rhizons>

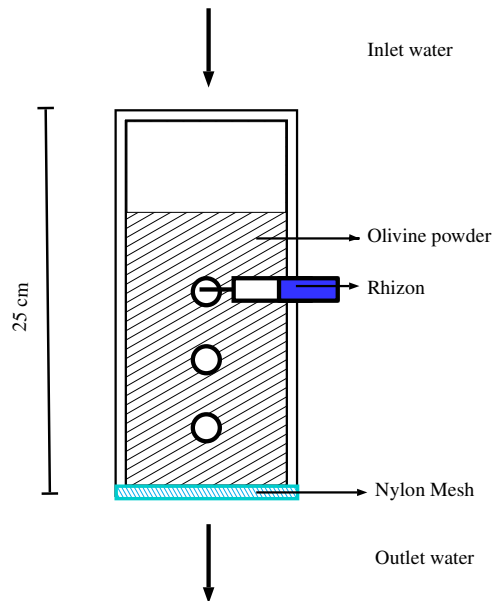


Figure 3.3: Illustration of the column design

Table 3.2: Mineral composition from XRF analysis (Keitzel, 2015)

Composition	Mass (%)
SiO ₂	40.14
Al ₂ O ₃	0.70
Fe ₂ O ₃	6.75
MnO	0.09
MgO	44.99
CaO	0.40
Na ₂ O	0.03
K ₂ O	0.06
TiO ₂	0.01
P ₂ O ₅	0.01
Loss on ignition	6.48
Total	99.68



Figure 3.4: Experimental setup showing arrangement of the columns containing olivine (1 to 3 are coarse, 4 to 6 are fine, and 7 to 9 are mixed), rhizones to collect pore water, and containers to collect outlet water.

Column	Grain-type	Weight (g)	TSA (m ²)
1	coarse	961.0	1018.66
2	coarse	984.3	1043.36
3	coarse	1003.6	1063.82
4	fine	630.3	6006.76
5	fine	676.1	6443.23
6	fine	660.0	6289.80
7	mixed	913.3	4835.92
8	mixed	881.3	4666.48
9	mixed	908.8	4812.10

Table 3.3: Physical characterisation of olivine in the columns with column number, grain-type, weight and total surface area (TSA)

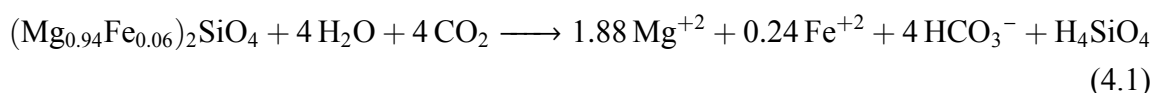
using a Metrohm™ Ion Chromatograph (IC) using a column that could identify Ca^{+2} , K^{+} , Mg^{+2} , Na^{+} , SO_4^{-2} , NO_3^{-} . All the concentrations were reported in $\mu\text{mol l}^{-1}$. The pH was measured using a WTW™ hand-held pH meter calibrated with three points using NIST buffer standards.

Chapter 4

Results and Discussion

4.1 Major ion analysis

The products of the dissolution reaction of olivine in an open system at ambient conditions are shown in Equation (4.1).



Mg: The outlet /effluent concentration of Mg, in $\mu\text{mol l}^{-1}$, is plotted against time (date), with intervals of one month; averaged for each grain-type (Figure 4.1). The concentration shows a power-law like decline for all three grain types. The fine and mixed release much more Mg than coarse in the first two months, the difference decreases over time and the pattern seems to show a slight reversal in the last month. The ratio of $[\text{Mg}^{+2}]$ in the outlet sample on the 30th and 160th day for fine : mixed : coarse is 8.2 : 5.5 : 1 and 1.5 : 1.2 : 1 respectively. The last measured value is around $350 \mu\text{mol l}^{-1}$.

Alkalinity: The reaction 4.1 shows that the dissolved CO_2 in the water appears as HCO_3^- in the solution. The Alkalinity is defined as the amount of bases than turn to an uncharged species upon acid addition. In natural environments, total alkalinity can be substituted with carbonate alkalinity which constitutes carbonate (CO_3^{2-}) and bicarbonate (HCO_3^-). Furthermore, through the Bjerrum plot¹, it can be shown that bicarbonate dominates in the pH range of 8 to 9. Thus, the total alkalinity can be taken as a good measure of the bicarbonate concentration in the system. The alkalinity is plotted with time (Date) in Figure 4.2. Fine and mixed grain types release more alkalinity than coarse in the first few months but the

¹The plot of equilibrium ratio of the various carbonate species in water to the pH

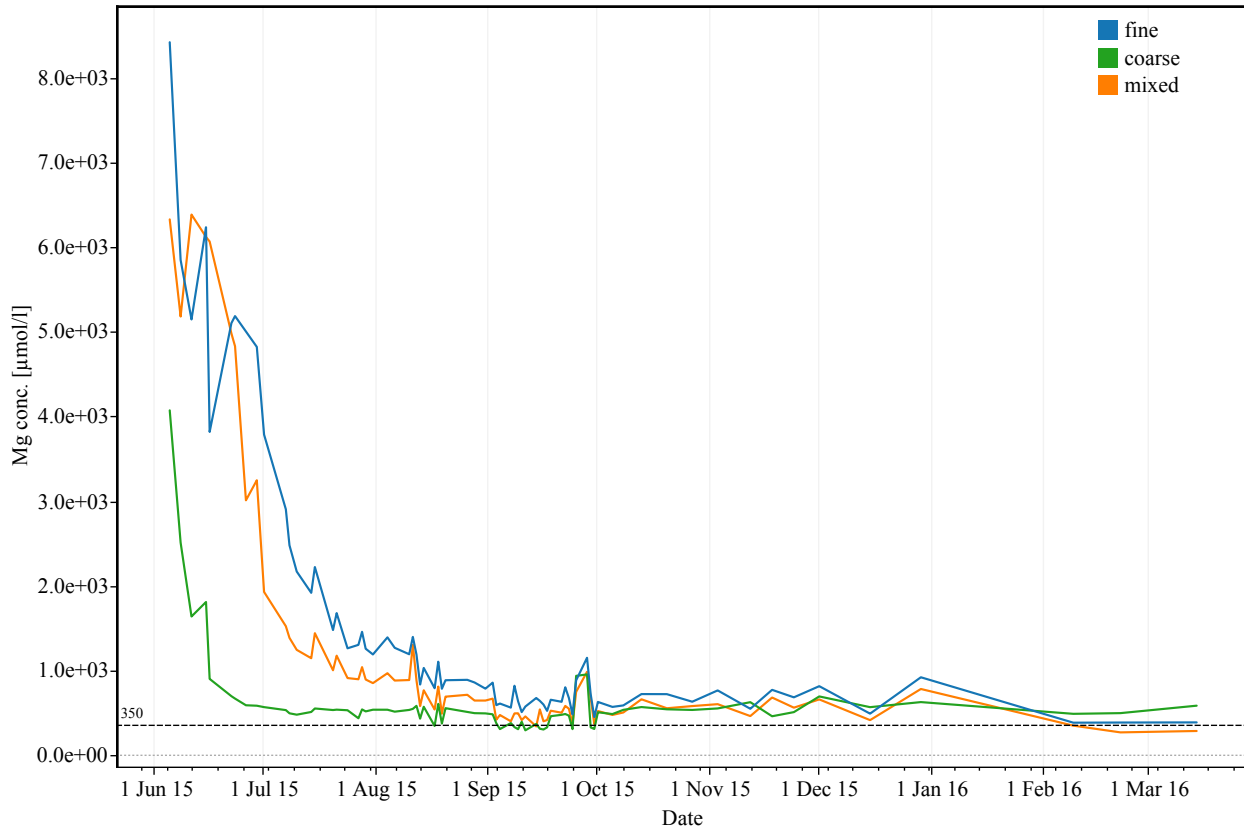


Figure 4.1: The outlet $[Mg^{+2}]$ plotted against the Time (Date), averaged for the three grain types- fine, coarse, and mixed.

ratio tapers down with time. The ratio of Alkalinity concentration in the outlet sample on the 30th and 160th day for fine : mixed : coarse is 5.5 : 2.8 : 1 and 2 : 1.75 : 1. The last measured values are around 850 $\mu\text{mol l}^{-1}$ and the alkalinity values for different grain types seem to be converging.

DSi: The outlet silica concentration is measured in terms of DSi $\text{Si}(\text{OH})_4$ (Figure 4.3). Unlike Mg^{+2} and Alkalinity, Si values show no significant trend. The last four months show less fluctuations compared to the first four months. Mixed particles release slightly more Si than fines or coarse, atleast in the last six months. In general, due to the high fluctuations it's best to say that the values stay within a range of 5 $\mu\text{mol l}^{-1}$ to 20 $\mu\text{mol l}^{-1}$. It may be of worth to point out that as the experiment progressed, white particles were observed at the base of the columns. The water seeping through the gap between the rhizon-hole and the rhizon flowed down the column, and overtime the water evaporated leaving the 'salts'/residue behind. Analysis of the residue showed presence of Silica. Thus, even though the outlet DSi values are low and thus the contribution of the Si outside might be significant, the total

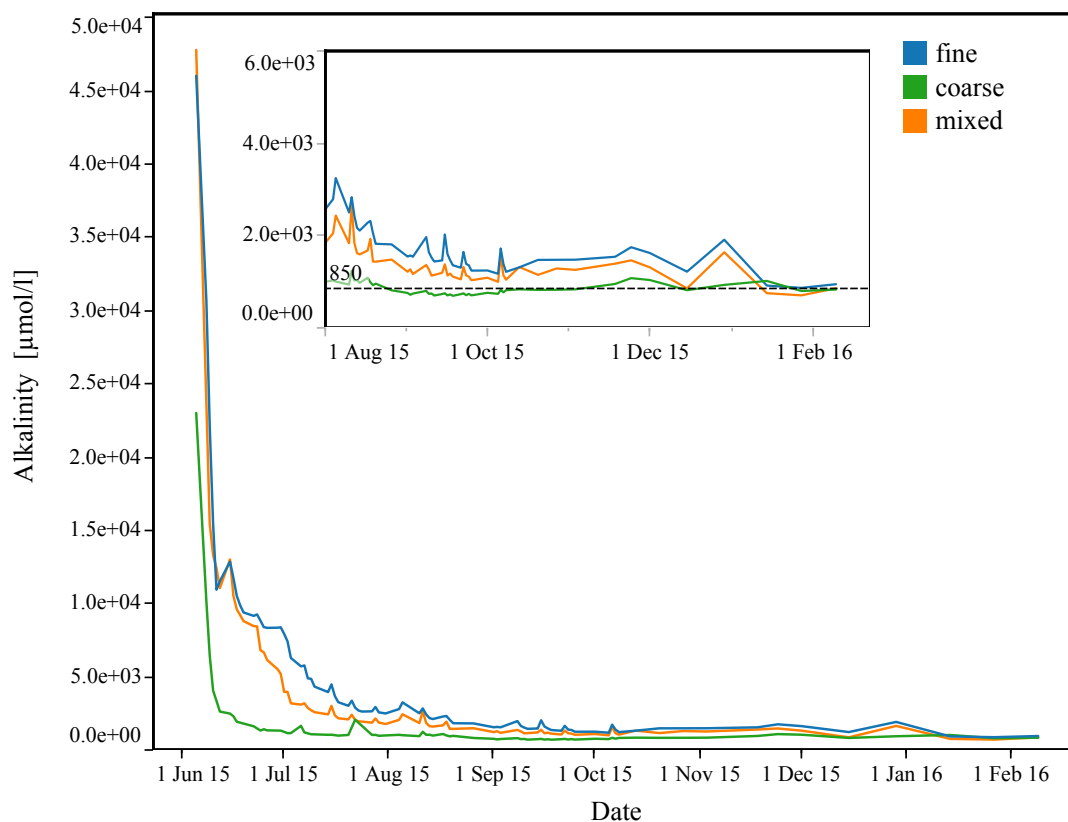


Figure 4.2: The outlet Alkalinity plotted against Time (Date), averaged for the three grain types- fine, coarse, and mixed.

water seeping through the gaps is very small and the overall affect can be neglected.

Mg/Si ratio: The ratio of Mg to the Si release is useful in knowing the state of the system and mechanism of the reaction. As previously discussed in section 2.5.1 forsterite shows apparent non-stoichiometric dissolution due to formation of a Si-rich layer on the mineral surface. The ratio of Mg/Si is plotted against Time (Date) in Figure 4.4 for the three grain types. The ratio increases in the first month and then sharply decreases for fine and mixed grain-type while coarse particles show a smaller drop which occurs earlier. The last measured value is around 40. A ratio of 1.88 would imply stoichiometric dissolution (see Equation (4.1)) and steady state conditions. Therefore, the current system is still far from steady-state which is unlike past experiments where steady state and stoichiometric dissolution was achieved within a few hundred hours (Hellmann et al., 2012; Pokrovsky and Schott, 2000; Wogelius and Walther, 1992).

The observation that outlet concentration profiles of Mg and Alkalinity ($\sim \text{HCO}_3^-$) are similar and $[\text{Alkalinity}] > [\text{Mg}^{+2}]$, follows from Equation (4.1). For every mole of forsterite

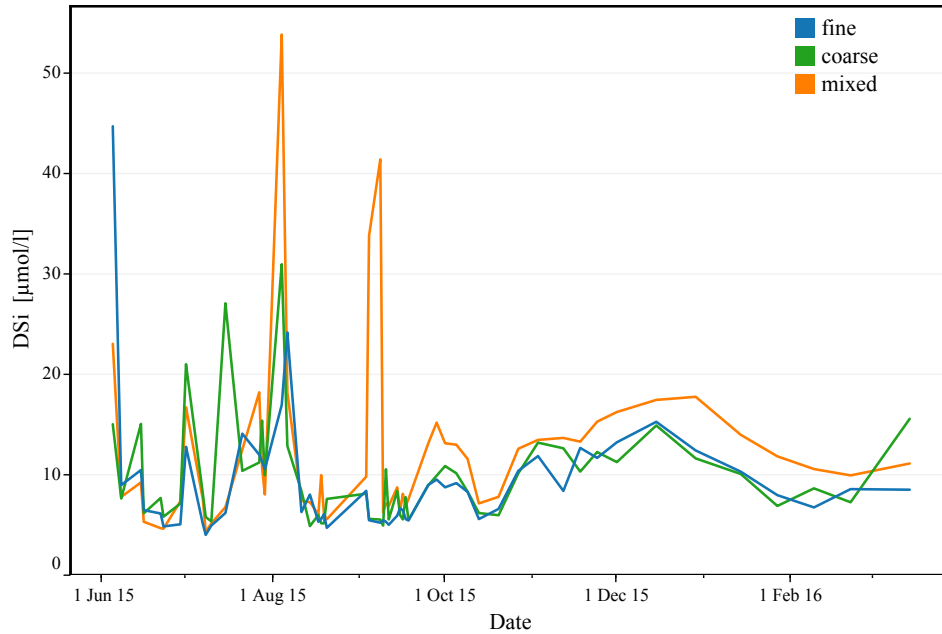


Figure 4.3: The outlet Dissolved Silica (DSi) plotted against Time (Date), averaged for the three grain types- fine, coarse, and mixed.

reacted, 1.88 mol of Mg^{+2} and 4 mol of HCO_3^- are produced. Silica doesn't show a similar trend due to reprecipitation and formation of Si-rich layer on the mineral surface. The preferred dissolution of fines or sites of high energy density are responsible for the high initial concentrations across the grain-types, especially for fine and mixed, which contain a higher percentage of them.

Minor ions: The XRF analysis indicates the presence of other metal oxides in the olivine. These oxides are present inside other minerals like chabazite, hornblende, chlorite, lazardite (Keitzel, 2015). The elements in these minerals are also released in the solution, though in minor quantities. These minerals may have an effect on the overall dissolution rate because of different rates of dissolution ((Schott et al., 1981) in Awad et al. (2000)). However, as forsterite is the dominant phase (Keitzel, 2015), and dissolves orders of magnitude faster than other minerals, the effect of the latter are expected to be insignificant ((Schott and Berner, 1985) in Awad et al. (2000)). The concentration of minor cations with time - Na^+ , K^+ , Ca^{+2} and minor anions - SO_4^{-2} , NO_3^- , Cl^- is shown in Section 6.6.

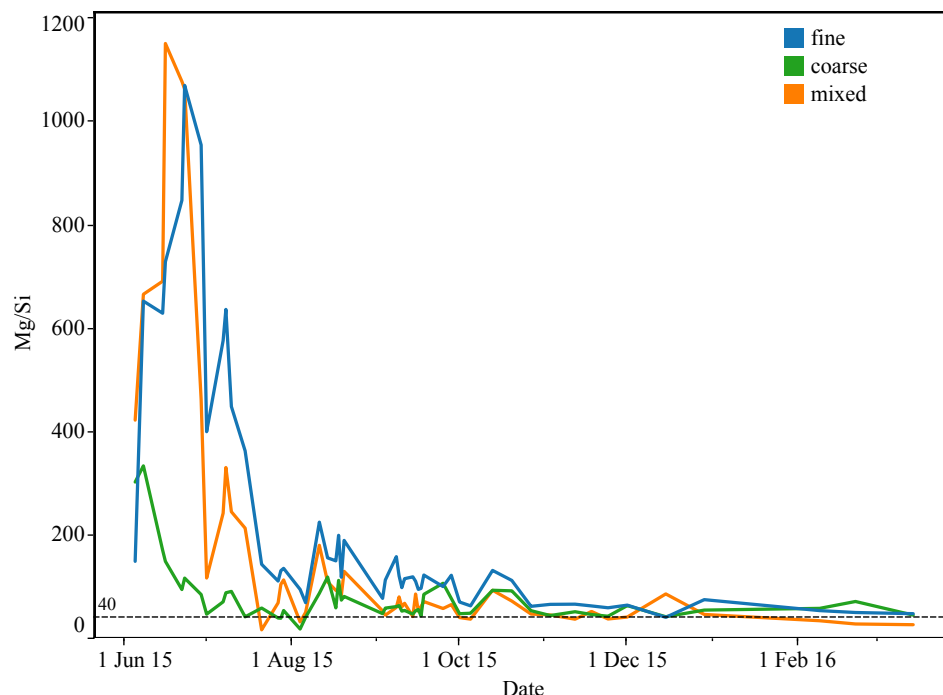


Figure 4.4: The ratio of Mg/Si plotted against time and averaged for the three grain-types — fine, coarse, and mixed.

4.2 Thickness of ‘surface layer’

The mechanism of formation of a Si-rich surface layer was discussed in section 2.5.1. Mg and Si are released stoichiometrically into the thin fluid layer surrounding the mineral but a part of the Si reprecipitates, leaving the other part as ‘observed Si’ in the bulk solution. At steady state, the rate of release of ‘observed Si’ equals the rate of precipitation so that the thickness of the Si-layer doesn’t change. Past experiments give the thickness of this layer to be around 1–5 nm (Hellmann et al., 2012; Pokrovsky and Schott, 2000). Calculations for the current experiment give the thickness in range of 0.2 nm to 0.5 nm (see Section 6.5) depending on the grain-type. These results reveal that the system hasn’t reached steady state, most of the Si-released is reprecipitated on the surface (leaving the ‘observed Si’ to be very small), and the thickness (T) follows the order $T_{coarse} > T_{fine} \sim T_{mixed}$.

4.3 Pore volume and Residence time

The olivine contained in all columns occupied the same volume at the start of the experiment. The pore volume and porosity was calculated for each column, see Equation (4.2), and is summarised in Table 4.1.

V_l (Pore volume) = Volume of cylinder containing olivine - Volume of olivine

$$V \text{ (Volume of cylinder)} = \pi \times r^2 \times h = \pi \times 2.8^2 \times 20 = 492.6 \text{ cm}^3$$

$$\text{Volume of olivine} = \frac{\text{mass of olivine (column 1)}}{\text{density of olivine}} = \frac{961.0}{3.32} = 289.46 \text{ cm}^3 \quad (4.2)$$

$$V_l = 492.6 - 289.46 = 203.14 \text{ cm}^3$$

$$\text{Porosity}(\phi) = \frac{\text{Pore Volume}}{\text{Volume of cylinder containing olivine}} = \frac{V_l}{V}$$

Column No.	Grain type	Pore Volume (cm ³)	Porosity
1	coarse	203.1	0.40
2	coarse	196.1	0.40
3	coarse	190.3	0.39
4	fine	302.8	0.62
5	fine	289.0	0.59
6	fine	293.8	0.60
7	mixed	217.5	0.44
8	mixed	227.2	0.46
9	mixed	218.9	0.44

Table 4.1: Table showing the pore volume and porosity for different columns.

The pore-space or the pore-volume of a packed bed is the portion of the total volume that isn't occupied by the solid material (Nimmo, 2004). The porosity (ϕ) is fraction of the total volume taken up by the pore space. The porosity depends on the particle-size distribution, particle shape, and the absolute particle-size (Zou et al., 2011). For particles smaller than $\sim 100 \mu\text{m}$, inter-particle forces, like vander-waals and electrostatic forces, become more important than gravity resulting in the formation of agglomerates or aggregates (Zou et al., 2011). Thus, even though the porosity within these aggregates is small, the overall porosity of column is large due to agglomeration. This might explain why coarser particles have higher porosity than fine or mixed grain type ($\phi_{\text{coarse}} > \phi_{\text{mixed}} > \phi_{\text{fine}}$, see Table 4.1).

The pore-volume is used to calculate the residence time (RT). The residence time, τ (seconds or days), is the average time spent by a water particle in a reservoir, and is calculated as the ratio of volume of reservoir to the flow rate of water. In column experiments with mineral dissolution, τ is the contact time between a mineral and a water sample. For the current experiment, the reservoir volume is the same as the pore-volume. The flow

rate is calculated by dividing the outlet volume (water exiting from the column) by $\sim 24 \text{ h}^2$. The residence time is calculated, as an example, for column 1 (coarse); the outlet volume is taken for the month of March (see Equation (4.3)). A similar calculation is performed for all months and grain-type and is plotted in Figure 4.6; the black line is the linear fit. It shows that absolute values of τ follow the order $\tau_{fine} > \tau_{mixed} > \tau_{coarse}$ at any point in time and $\frac{d\tau_{fine}}{dt} > \frac{d\tau_{mixed}}{dt} > \frac{d\tau_{coarse}}{dt}$. Equation (4.3) shows that τ depends on the pore-volume and the outlet flow rate (F_l). The development of F_l with time (Date) is shown in Figure 4.5; the black line represents the linear fit. Assuming the pore volume to be constant with time, the higher initial τ for fine compared to coarse can be explained on the basis of the higher pore volume of fine compared to coarse (initial F_l is almost the same), but as the experiment progresses, the changes in flow rate start playing an important role in shaping the residence time, i.e., a decrease in flow rate increases the residence time.

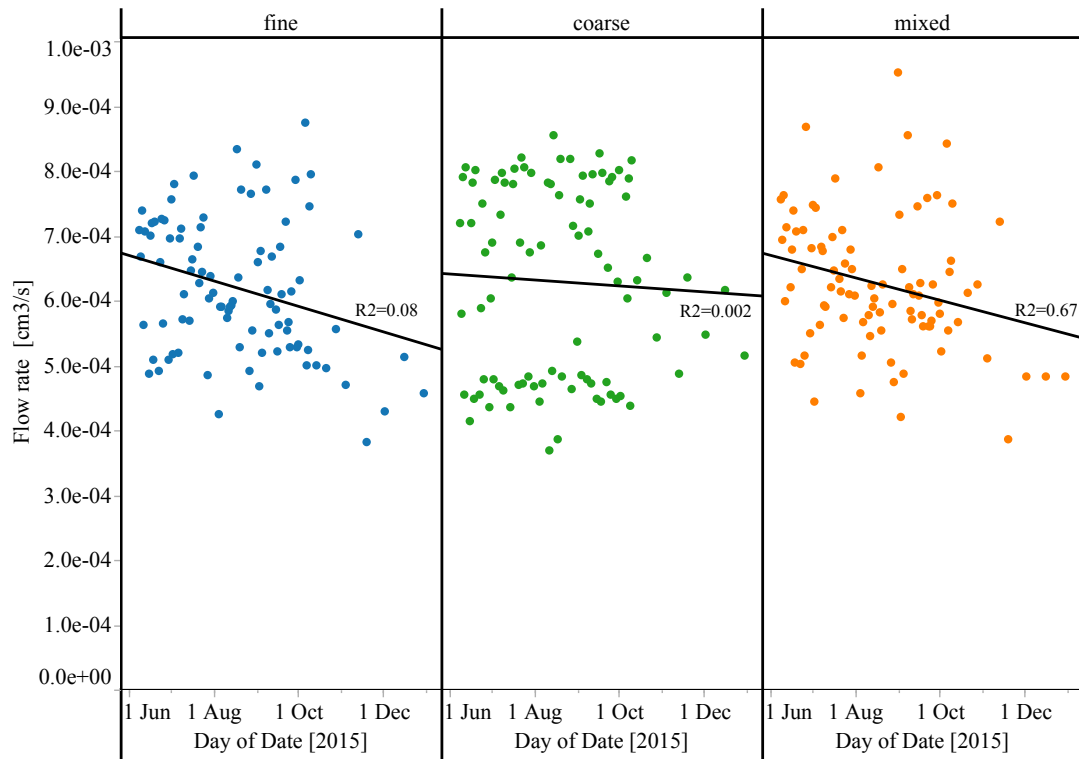


Figure 4.5: Flow rate (cm^3s^{-1}) vs. Time (Date). The results are averaged for the three grain types- fine, coarse, and mixed. The black line is the linear fit. R^2 is the regression coefficient.

²The water collected from the rhizons leads to fluctuations in the outlet volume. This water cannot be added to the outlet volume because it is forced out of the system. Since the rhizon sampling was done on specific days, one could remove the outlet volume from the following day in the calculation of residence time for consistency. This changes the residence time over the experiment duration, but the general trend is unaffected— τ_{fine} increases the most, τ_{coarse} remains almost the same and τ_{mixed} shows an increase which is smaller than fine.

The changes in flow rate of the fluid are harder to quantify. The fluid flow velocity u_c is calculated as flow rate divided by the cross-sectional area of the bed, and has been shown to depend on fluid viscosity, pressure difference across column, length of the column, porosity, surface of the column per unit volume of bed, specific surface area (per volume), tortuosity, and shape and size of particles (Coulson et al., 1991). These factors are not further discussed in this work.

$$F_l \text{ (outlet flow rate)} = \frac{\text{Outlet volume}}{\text{time}} = \frac{68.21 \text{ cm}^3}{(24 \times 60 \times 60) \text{ s}} = 7.9 \times 10^{-4} \text{ cm}^3 \text{ s}^{-1}$$

$$\tau = \frac{V_l}{F_l} = \frac{203.14 \text{ cm}^3}{7.9 \times 10^{-4} \text{ cm}^3 \text{ s}^{-1}} = 2.57 \times 10^5 \text{ s}$$
(4.3)

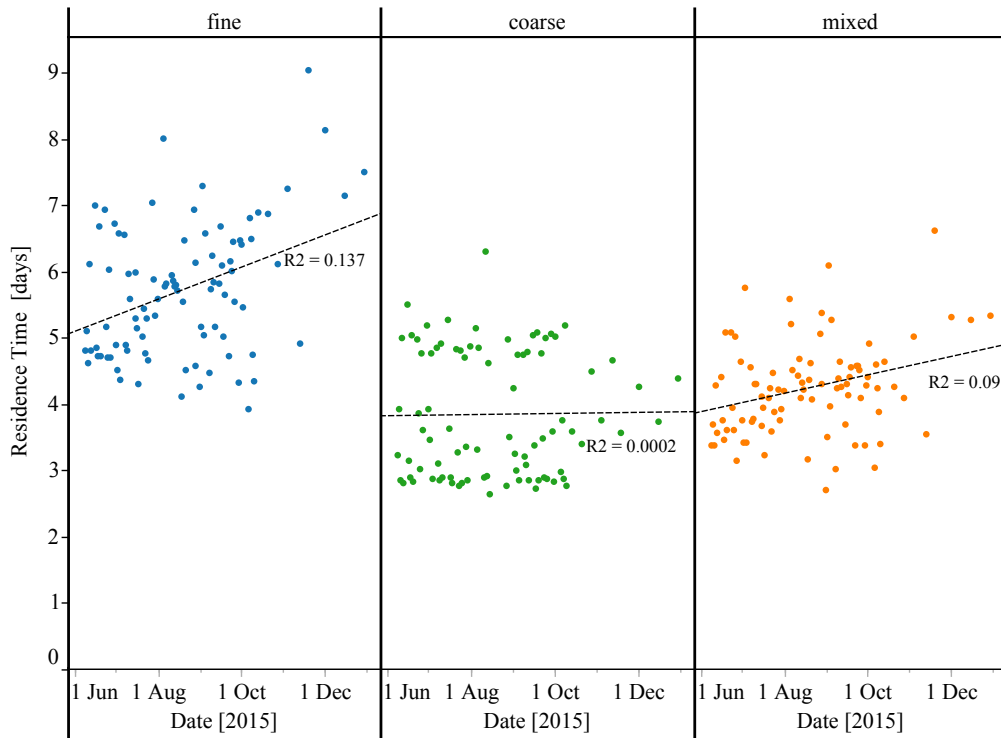


Figure 4.6: Residence Time (days) plotted with the progress of the reaction (Date), for the three grain types— fine, coarse, and mixed. The black line is a linear fit and shows the general trend. R^2 is the regression coefficient.

4.4 Rate of Reaction

The reaction rate is calculated as the release rate of products into the solution. As an example, for column # 1 and Mg^{+2} (observed in March) the rate is calculated as:

$$R_{Mg} = \frac{[\Delta Mg] \times \text{outlet volume}}{\tau \times TSA} \quad (4.4)$$

$$R_{Mg} = \frac{(546 \times 10^{-6} \text{ mol l}^{-1}) \times (68 \times 10^{-3} \text{ l})}{(2.57 \times 10^5 \text{ s}) \times (1018 \text{ m}^2)} = 7.57 \times 10^{-14} \text{ mol m}^{-2} \text{ s}^{-1} \quad (4.5)$$

where,

τ = residence time of water in column, s

TSA = Total surface area of particles, m^2

V_l = Pore volume, l

The rate of release of Alkalinity and DSi is similarly calculated. The combined results are shown in Figure 4.7. In general they follow a trend similar to that of concentration (see Figures 4.1 to 4.3). R_{Mg} and R_{Alk} decrease with time, for all grain-types. The decrease is fastest in the first four weeks of the experiment. R_{DSi} shows no particular trend and seems to stay between a range of values. The rate of reaction measured for Mg, Alkalinity, and DSi follows the order: $R_{Alk} \sim R_{Mg} > R_{Si}$. The rate of reaction is higher for coarser particles than fine particles, and fine and mixed particles show similar values, i.e., $R_{Mg_{coarse}} > R_{Mg_{fine}} \sim R_{Mg_{mixed}}$. A similar observation is seen for R_{Alk} and R_{Si} .

The decrease in R_{Mg} and R_{Alk} (see Figure 4.7) could be explained by two separate factors. Intrinsic factors are related to the physical and chemical properties of the mineral and how they change with time. These factors are enclosed within TSA in Equation (4.4). The decrease in reaction rate with time, observed in previous experiments, has been attributed to the fast dissolution of fine particles or sites of high surface energy (Brantley, 2008a). The olivine rock in this work also contains fines and sites of high energy density (created during grinding and crushing) and thus, their fast dissolution too could partly provides an explanation. Furthermore, BET surface area measured, for fine grains, one year after the start of the current experiment show a $\sim 15\%$ increase in surface area (Table 6.2). White and Brantley (2003) in long-term columns experiments with granite suggested that at-least a third of the decrease in their observed reaction rate with time was due to increases in physical surface area. In conclusion, intrinsic factors- reduction in energetic sites and in-

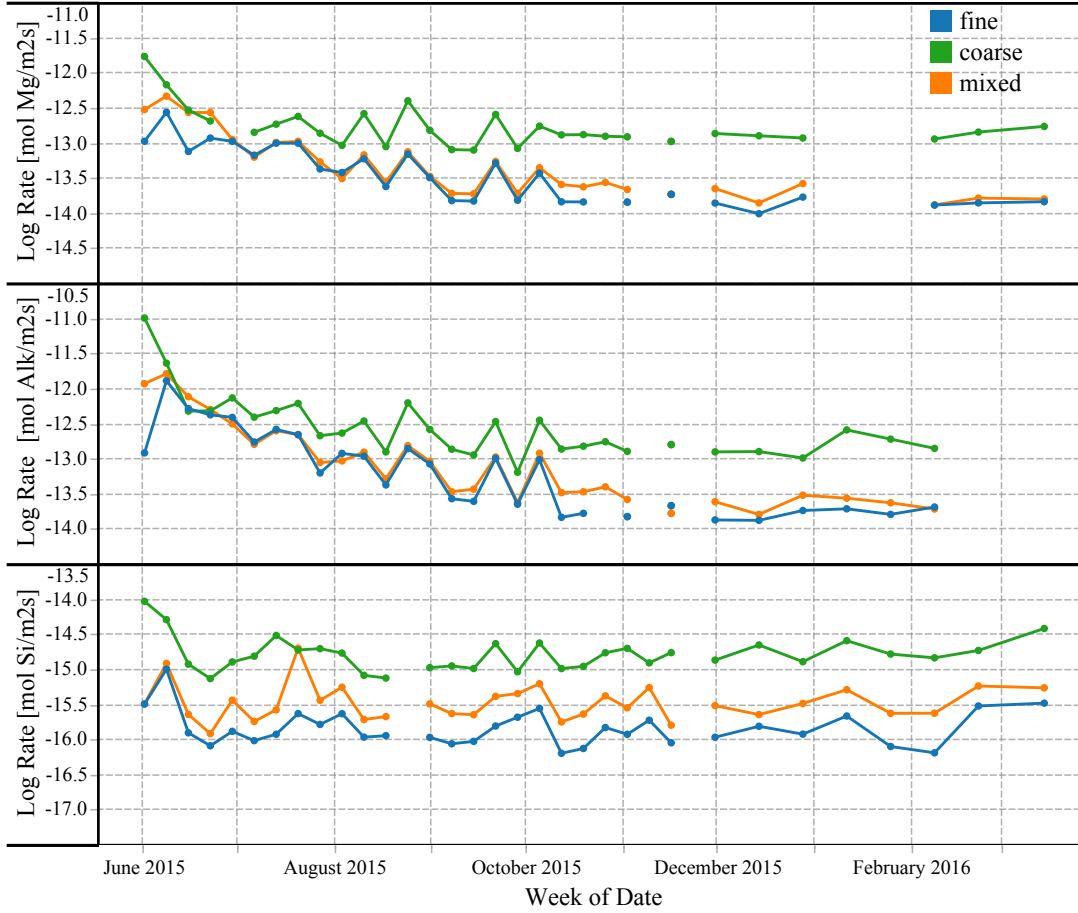


Figure 4.7: The rate of reaction in terms of Mg, Alkalinity, and DSi (in $\text{mol m}^{-2} \text{s}^{-1}$) plotted against Time (Date), averaged for the three grain types— fine, coarse and grain and over week.

crease in physical surface area, at least partly contribute to the decrease in reaction rate with time. Extrinsic factors, on the other hand, like hydrology, solute composition are external to the silicate mineral and are more difficult to understand (White and Brantley, 2003). In Equation (4.4), these terms are ΔMg , residence time τ , and outlet volume. As shown and discussed in the previous section, in general, τ increases with time, $[\text{Mg}^{+2}]$ decreases with time, and outlet volume decreases with time (F_l is outlet volume divided by time). When these effects are considered independent of each other they could also explain the observed decrease in reaction rate. In summary, both intrinsic and extrinsic factors control reaction rate though the relative importance of each cannot be exactly quantified.

Another reason could be the flushing out of particles from the column ($<20 \mu\text{m}$) (the aperture of the nylon sieve at the bottom of the columns is $20 \mu\text{m}$), or their complete dissolution in the initial phase. Since these particles contribute to a significantly to the rate, the escape or reduction of a tiny fraction could lead to a reduction in overall rate. No tests

were unfortunately performed to find this.

It is also observed in Figure 4.7 that R_{Mg} is almost two orders of magnitude greater than R_{DSi} . The difference in release rates during silicate dissolution can be due to incongruent or non-stoichiometric dissolution, difference in stoichiometric amounts of elements present in minerals, or both (Rimstidt et al., 2012). The different release rates in this experiment are because of the apparent incongruent dissolution due to formation of a surface layer (see section 2.5.1 for explanation and almost all Si released is precipitated - Section 6.5) as well as the different stoichiometric contribution (see equation (4.1)). The large difference in rates means that the former process dominates.

The columns with coarser grain-type show almost an order of magnitude higher reaction rate than fine and even mixed grain-type (see the average over last months in figure 4.7). Generally at any time t , $\Delta Mg_{fine} > \Delta Mg_{coarse}$, $F_{l,fine} < F_{l,coarse}$ (F_l is taken as proxy for outlet volume), $\tau_{fine} > \tau_{coarse}$, $TSA_{fine} > TSA_{coarse}$. The first two terms are directly proportional to rate while the last two are inversely proportional to rate. Thus, if the absolute difference in Mg is not higher than the absolute differences of F_l , τ , and TSA , coarse particles would have a higher rate than fine particles.

4.4.1 Rate comparison with literature

The observed reaction rate is compared with previous forsterite dissolution experiments. The compilation of previous experiments at 25 °C was done by Rimstidt et al. (2012). They summarise that almost all past experiments reached congruency and steady-state, therefore, the difference in release rates of Mg and Si were only due to stoichiometry effects. Figure 4.8 shows the plot of R_{Mg} from Rimstidt et al. (2012) normalised to BET surface area) against pH. To get an estimate of the rate difference, the past rate data is compared at pH 8 (see figure 4.9) with R_{Mg} , R_{Alk} , R_{DSi} from figure 4.7, even though the current experiment hasn't reached steady state. The latter are averaged from the last few months of the experiment. A range of the rate is presented to account for the difference across columns/grain-types. The upper and lower bounds are coarse and fine grain-type respectively. Thus, depending upon which element and which grain type is taken, R_{Mg} , R_{Alk} are ~ 3 orders of magnitude, and R_{DSi} is ~ 4 orders of magnitude smaller than past experiments.

Past dissolution experiments were conducted under similar conditions in closed MFRs and BRs - at 25 °C, with very low rock to volume ratio, pre-treatment of grains to remove fines, sample containing almost uniform grain-size, and run time of few hundred hours. The current experiment on the other hand is a column experiment, with high-rock to volume ratio conducted without pre-treatment to remove fines, and rates observed over long time

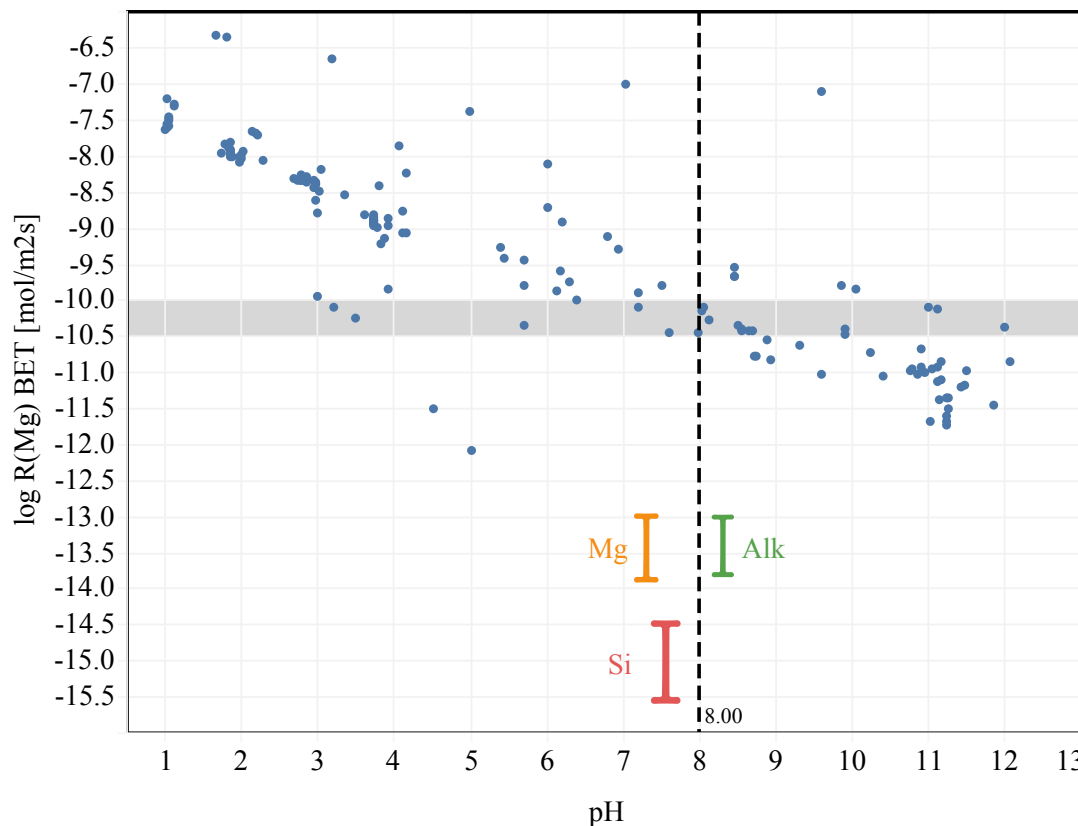


Figure 4.8: Rate data (in terms of $\log r_{BET} \text{ Mg}^{+2}$) vs. pH from past experiments on forsterite dissolution (Rimstidt et al., 2012). The black line is the pH of interest. The range of Mg, Alkalinity, Si rates shown in orange, green, and red respectively.

period. Thus, the comparison of reaction rate with literature is only possible when common factors affecting rate have been proven to not have influenced the rate. The factors affecting rate in surface-controlled reactions were discussed before in section 2.5.3.

1. **pH and temperature:** Unlike previous laboratory experiments which control system pH by changes in concentration of acids like H_2SO_4 or HCl (see Table 1, (Rimstidt et al., 2012)), no such control was done in this experiment. The inlet water (in equilibrium with the atmosphere and at pH 5.7) is assumed to immediately turn alkaline upon contact with the first layer of olivine and remain constant throughout the column. This assumption is supported by previous experiments where a reactor containing water immediately turned alkaline upon addition of few grams of olivine (Martinez et al., 2014; Tobiesen, 2016). Assuming the conditions in column to have a higher pH, say 9 (which lead to lower rate, see figure 4.8) one cannot still explain the large difference observed between observed and past values.

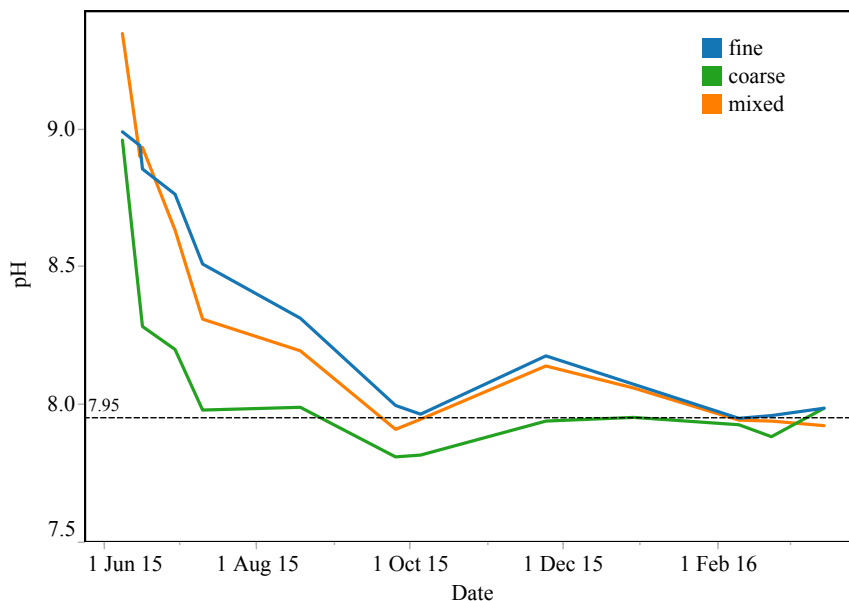


Figure 4.9: pH of the outlet water plotted against Time (Date) for the three grain types — fine, coarse, and mixed.

The effect of temperature on reaction rate is found by using Equation (2.10). The rate difference at 20 °C and 25 °C is ~ 0.1 log units. Thus, even assuming the experiment temperature to be a few degrees lower than 25 °C, it alone cannot explain the difference.

2. **Total surface area:** The contribution of the ultrafine grains ($<10 \mu\text{m}$) to the specific surface area is almost 97 % and 90 % for the coarse and fine grain type respectively (see Section 6.4). Section 4.4 discussed the possibility of losing these ultrafines. Only one BET measurement was performed one year after the start of the experiment; the sample taken from the top of the column. This indicated an increase in SSA and would point that no ultrafines were lost during the experiment. Even though this result could be different for particles closer to the very end of the column, this effect is assumed to be small compared to the total column.

Most dissolution experiments are performed in MFRs and BRs, with agitators moving few grams of the mineral in a fluid medium. This wets the entire mineral surface and all grains are more or less equally wetted. The ‘wetted area’ can be defined as the area of the mineral in contact with the fluid. In column experiments with high rock to volume ratio, neither the complete surface of a single grain nor different grains are uniformly wetted. This could be due to many factors - formation of dead zones (regions where water remains stagnant or doesn’t reach at all), preferential flow (water

seeps through fractures and cracks without interacting with many grains), compression and stacking of particles, and aggregation of fine particles. When BET values are used, unaccounting for these factors could lead to overestimation of the ‘actual and available surface area’. This is different from assuming the effective surface area to be same as BET surface area (see section 2.5.3). In fact, the concept of wetted surface area brings another layer of complexity in finding the ‘actual surface area’ which takes part in the reaction.

Assuming the ‘actual surface area’ to be, say, 20 times smaller than BET surface area, would lead to a 1.3 log units reduction in measured rate, and thus this factor alone cannot account for the observed rates.

3. **Effect of reaction products, $p\text{CO}_2$** As already discussed, the concentration of reaction products or dissolved CO_2 don’t significantly or conclusively lead to change in dissolution rate.

Any of the factors taken alone cannot explain the observed dissolution rates. Even assuming a combination of the higher end of rate values for each factor, it wouldn’t explain more than half of the difference observed. Thus, common factors that usually influence surface-controlled rate don’t explain the observed results. Furthermore, a surface-controlled rate would mean that the rate is independent of particle size, which is contradictory to observation. These results leave the possibility of the reaction rate to be transport-controlled or a mixture of transport and surface control, and will be discussed in the next section.

4.4.2 Transport control in column reactors

To get an estimate of the reaction rate in a packed bed and of forsterite and the factors controlling it, a theoretical model of Rimstidt (2015) is used. This model includes diffusion and surface reaction equations. Before the reaction occurs at the mineral surface, the reactant, H^+ ions, must move from the bulk of the fluid across a static thin fluid film to the surface. This movement, called diffusion flux, is driven by the concentration gradient across the film. The values of the diffusion flux (J_D) and reaction flux (J_R) decide what controls the overall reaction rate. Both are calculated normalised to geometric surface area. The model thus explores how mineral dissolution in a packed bed is affected by flow rate, grain diameter, diffusion coefficients, and temperature (Rimstidt, 2015). The equations for

J_D and J_R are given in Equation (4.6).

$$J_D = k_D(c_s - c) \quad (4.6)$$

$$J_R = -k_R c_s \quad (4.7)$$

where k_D is the diffusion coefficient, c_s is the $[H^+]$ at the surface, c is the bulk $[H^+]$, k_R is the rate constant of the reaction.

The diffusion coefficient is further defined as:

$$k_D = 1.17 \left(\frac{Lq}{\nu} \right)^{-0.42} \left(\frac{D}{\nu} \right)^{\frac{2}{3}} \quad (4.8)$$

where L is the particle diameter (m), q is the Darcy velocity ($m s^{-1}$), ν is kinematic viscosity ($m^2 s^{-1}$), D is the diffusion coefficient of the aqueous species ($m^2 s^{-1}$).

The model is slightly modified to account for the higher pH in the current experiment (Rimstidt only showed results for pH <5.6). The model rates are steady-state in terms of the reactant, H^+ , and have been modified through stoichiometry to obtain release rates of products — Mg^{+2} (adding log 0.5 = - 0.3 to H^+ release rates) and Si (adding log 0.25 = - 0.6 to H^+ release rates). The model doesn't account for pCO_2 affects. The variables entered into the model are summarised in Table 4.2. The Darcy velocity, q , is the volumetric flow rate divided by the cross-sectional area transited by the flow. The grain diameter, L , is taken as the mean of the grain size distribution obtained by laser-granulometry.

Grain type	Darcy velocity, q ($m s^{-1}$)	Grain diameter, L (μm)	pH
Fine	2.8×10^{-7}	25	8
Coarse	1.68×10^{-5}	680	8

Table 4.2: Variables pertaining to the current experiment entered into the model of Rimstidt (2015).

The results are summarised in Figure 4.10. At the temperature of interest $J_D \ll J_R$ by almost four orders of magnitude. Thus, the reaction rate is diffusion-controlled. Further, coarse particles have a higher (0.5 log units) rate than fine particles which is due to different particle diameter and Darcy velocity (see Equations (4.6) and (4.8)).

In order to compare the model and experimental results, the BET normalised surface rates of the experiment are converted to geometric surface rates by dividing the former by a factor of 5 (or adding 0.7 log units to the rate term in Equation (4.4)) (see Rimstidt et al. (2012) for discussion on roughness factor). The rates are presented as a range due to

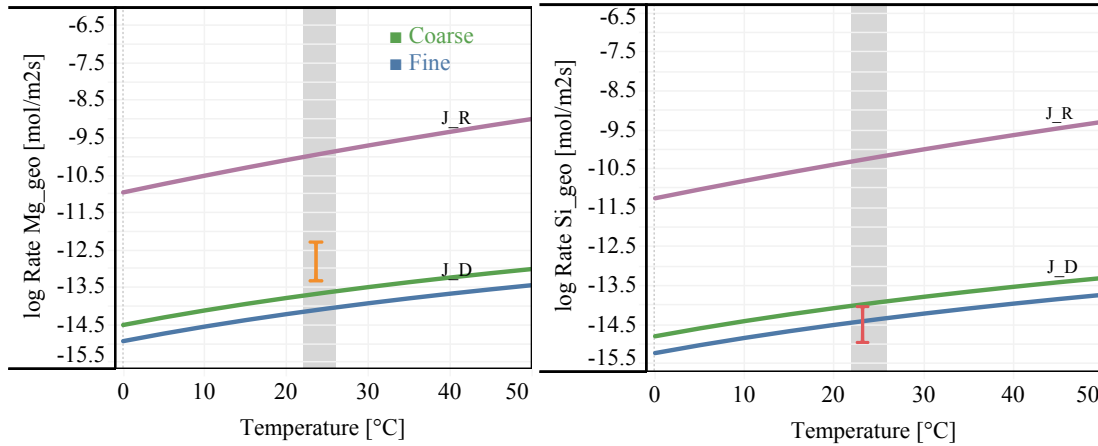


Figure 4.10: Plot of Log Rate of dissolution (in $\text{mol m}^{-2} \text{s}$), vs. Temperature ($^{\circ}\text{C}$) at pH 8. The purple curve is the reaction flux (J_R) and is the same for fine and coarse grain types. J_D is the dissolution flux for fine (green) and coarse (blue). The green and red bar are the range of measured values for Mg and Si respectively. The grey band is the temperature range of interest.

difference in rates across grain-type. The experimental rate is about one to two orders of magnitude larger than model results for Mg but almost the exact range for Si (Figure 4.10). It's worth mentioning that the current experiment hasn't reached steady state while the model results assume steady-state. This means that experimental results will decrease in the future though extremely slowly.

Another process could explain the one to two order difference, between experimental and model results, observed for Mg. As each column is watered, the water doesn't immediately trickle down the column but stays at the top for some time. The amount and time of this over-head water increased as the experiment progressed. This means that the thin layer, a few grams, of olivine at the very top may react faster (with a value J_R) than the rest of the column because it is in contact with a comparatively large amount of water. This could explain the higher rate observed for Mg. A corresponding higher rate is not observed for Si because of the formation of a Si-rich layer around the mineral surface.

Chapter 5

Conclusions, Implications, and Future Work

To assess the potential of enhanced weathering as a method to sequester CO₂, knowledge of the reaction rate of a silicate, e.g., forsterite, is needed. Past experiments on forsterite dissolution might not be suitable to answer this due to the conditions and setup under which they were performed. The current experiment fulfills this gap by undertaking long term packed-bed column experiments, open to atmosphere and without sample pre-treatment. The columns are separately filled with three different size fractions - coarse, fine, and mixed grain-type, and water is poured over them.

After running for almost one year results show that the olivine hasn't reached steady-state, which might be due to the presence of a large amount of fines in the column. The rate differs across the measured species - $R_{Alk} \sim R_{Mg} > R_{Si}$ due to reprecipitation of released Si as a Si-rich surface layer. The measured rate is many orders of magnitude lower than observed in past literature, and coarse grain-type having higher rate than fine and mixed. These results cannot be understood when rate is surface-limited, normally assumed in forsterite dissolution. The experiment results are further compared with a theoretical rate model for packed-bed. The model-results show transport controlling the reaction rate; which are lower than observed for Mg but in agreement for Si. This could be explained assuming the rate to be surface-controlled, thus faster, in the first few layers followed by transport-control in the rest of the bed. In conclusion, results from past laboratory experiments cannot be directly used to estimate CO₂ absorptive potential or to manipulate rate for EW application; because the system could become transport-controlled.

Weathering rates measured in the laboratory have been found to be orders of magnitude greater than those observed in the field. The results from this study show that this could at least partly be explained based on transport-control; as column experiments better mimic

natural conditions.

Other processes could influence olivine dissolution rates in nature, for e.g., the high $p\text{CO}_2$ in soils through soil respiration processes, presence of complex ligands, role of soil bacteria etc. Even though the current experiment doesn't consider them, it puts forth a step in the right direction; of estimating field weathering rates and its influencing processes. Lastly, surface area is an important property affecting rate, and BET surface area shouldn't be substituted for the 'actual and available surface area'; for it hinders rate comparability across experiments and introduces sources of uncertainty. A novel method must be found out to move past this problem.

Chapter 6

Appendix

6.1 Climate Engineering and CDR options

Geo-engineering is defined as the deliberate large-scale intervention in the Earth's climate system to moderate global warming (Shepherd, 2009). Geo-engineering methods can be divided into two categories: Carbon dioxide removal (CDR) techniques which sequester atmospheric CO₂ or prevent release of CO₂, and solar radiation management (SRM) techniques that reflect a small percentage of the Sun's radiation back into space, causing the Earth to absorb less solar radiation, and eventually cool. Figure 6.1 illustrates possible technologies and the region of application (land, ocean, atmosphere). Enhanced weathering is not explicitly mentioned but comes under *Alkalinity Addition*.

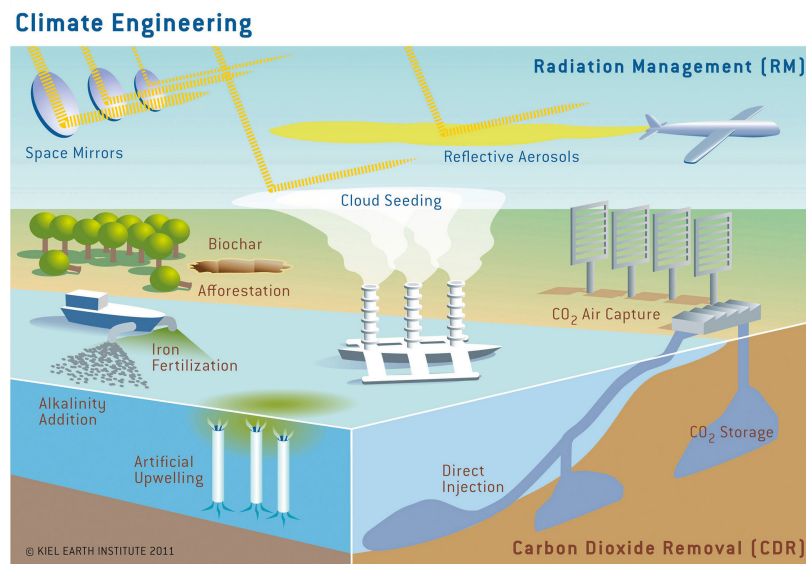
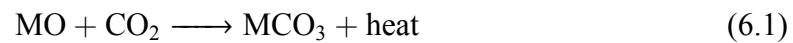


Figure 6.1: Schematic illustration of CE technologies. Source: kiel-earth-institute - own work, <https://commons.wikimedia.org/w/index.php?curid=38682676>

6.2 Enhanced Weathering and Mineral Carbonation

Mineral carbonation is another method of carbon sequestration and involves the reaction of a near-pure stream of CO₂ (coming from the capture-stage of a power plant) with metal oxide bearing minerals to form insoluble carbonates. This process can be *in-situ* where CO₂ is pumped into geologic sites containing silicate rocks or *ex-situ* where rocks are mined, crushed, and then reacted with a CO₂ stream at high- temperature and pressure (Coninck et al., 2005). An example of general carbonation reaction is shown in equation (6.1), CO₂ reacts with metal oxides (indicated here as MO, where M is a divalent metal, e.g., calcium, magnesium, or iron) to form the corresponding metal carbonate and give heat.



The differences between mineral carbonation and enhanced weathering are shown in Section 6.2.

	Enhanced Weathering	Mineral Carbonation
Conditions	CO ₂ dissolved in water reacts with mineral at ambient temperature and pressure	CO ₂ gas-stream reacts with minerals at elevated temperature, pressure or both
CO₂ source	Atmosphere	Near-pure CO ₂ stream from capture-stage of power plants/industries
Reaction products	Dissolved metal cations, silica, trace carbonates	Metal carbonates and silica

Table 6.1: Summary of main differences between Enhanced weathering and Mineral carbonation

6.3 Molecular formula of olivine

$$\text{wt. \% of Fe in Fe}_2\text{O}_3 = \frac{\text{Molecular Wt. of Fe}}{\text{Molecular Wt. of Fe}_2\text{O}_3} = \frac{56}{120}$$

$$\text{mol \% of Fe} = \frac{\text{wt. \% of Fe in Fe}_2\text{O}_3 \times \text{wt. \% of Fe}_2\text{O}_3}{\text{molecular mass of Fe}} = \left(\frac{56}{120}\right)\left(\frac{6.75\%}{56}\right) = 0.05625$$

$$\text{wt. \% of Mg in MgO} = \frac{\text{Molecular Wt. of Mg}}{\text{Molecular Wt. of MgO}} = \frac{24.3}{40.3}$$

$$\text{mol \% of Mg in sample} = \frac{\text{wt. \% of Mg in MgO} \times \text{wt. \% of MgO}}{\text{molecular mass of Mg}} = \frac{24.3 \times 44.99}{40.3 \times 24.3} = 0.8957$$

$$\text{Molar ratio} = \frac{\text{Mg}}{\text{Fe}} = \frac{0.8957}{0.05625} = 15.92$$

$$\frac{x}{1-x} = 16.92$$

$$x = 0.941$$

Therefore, the chemical formula is $\text{Mg}_{1.88}\text{Fe}_{0.12}\text{SiO}_4$

6.4 BET analyses

The specific surface area (SSA) of a mineral surface is found using a method developed by Brunauer–Emmett–Teller (BET) ([Brunauer et al., 1938](#)). It involves the adsorption of an inert gas, such as nitrogen, to the mineral surface at low temperature; forming a mono-layer thick film. The change in N_2 pressure is measured and the corresponding gas adsorbed is calculated ([Brantley and Mellott, 2000](#); [Rimstidt, 2013](#)). The total surface area (TSA), also called BET surface area ([Brantley \(2008a\)](#)), is calculated by multiplying the specific surface area with the sample weight.

Two surface area analyses were performed for each of the two grain types, i.e., $<63\ \mu\text{m}$ and $0\text{--}3\ \text{mm}$. No chemical pre-treatment was done on the samples, but they were heated in near-vacuum conditions at a rate of $5\ ^\circ\text{C min}^{-1}$ to $300\ ^\circ\text{C}$ and held at that temperature for 120 min to remove adsorbed water. For each analysis, 5–6 g of the sample was taken in a long-necked tube, cleaned with acetone and dried overnight in an oven at $50\ ^\circ\text{C}$, with a stem diameter of 12 mm and a rounded bulb at the bottom. The inclusion of bigger grain particles ($>2\ \text{mm}$) from the coarse grains could have been limited because of the method of sample addition into the test tube. The results are shown in table [6.2](#).

Sample	Date	SSA (m ² g ⁻¹)	Sample mass (g)
0–3 mm	03.03.2015	0.979	5.35
0–3 mm	04.03.2015	1.16	5.3
<63 µm	09.03.2015	10.082	6.01
<63 µm	11.03.2015	9.471	5.02
<63 µm	14.12.2016	11.305	5.288

Table 6.2: BET measured specific surface area for the two grain types- fine and coarse.

To find the contribution of the ultrafines (<10 µm) to the overall SSA, as well as validate the measured SSA, results were compiled from [Brantley and Mellott \(2000\)](#); [Rimstidt et al. \(2012\)](#); [Moosdorf et al. \(2014\)](#) and plotted as SSA versus mean particle diameter (see Figure 6.2, the axes have a logarithmic scale). The averaging method of [Tester et al. \(1994\)](#) was used to find the mean particle diameter; which assumes a flat size distribution between the size-range of particles ([Rimstidt, 2013](#)). Regression analysis gives the following relation:

$$SSA = 60.39(D)^{-1.237} \quad (6.2)$$

The range of particle diameters (D) and their weight fraction, for the coarse and fine grains in the current experiment, are available from laser-granulometric measurements (see Figures 3.1a and 3.1b). For each range, the mean diameter was calculated using methodology of [Tester et al. \(1994\)](#)¹.

Using Equation (6.2), the SSA for each mean particle diameter D is calculated, and then multiplied by the weight fraction to get its surface area. Summing across all of surface areas gives the expected SSA of the sample (see Tables 6.4 and 6.5) .

The contribution of each particle fraction to the total of the surface areas is shown in Figure 6.3, for fine grain-type. Particle fractions in the 0–10 µm range contribute ~90 % of the total of the surface area but only ~33 % of the total weight. The same particle fraction for coarse contribute ~97 % and ~1 % respectively (not shown here). This highlights the important role of ultrafines in the fine and coarse grain-type.

The total of the surface areas, marked in bold in Figure 6.3, is an estimate of the SSA of the grain-type. The values obtained for the fine and grain-type don't significantly differ from the measured BET values (Table 6.3) .

¹The last sieve size for coarse particles 0.5–18 µm was not averaged by this method since tiny changes in its value resulted in huge changes in calculated surface area. It is taken as 0.5 µm

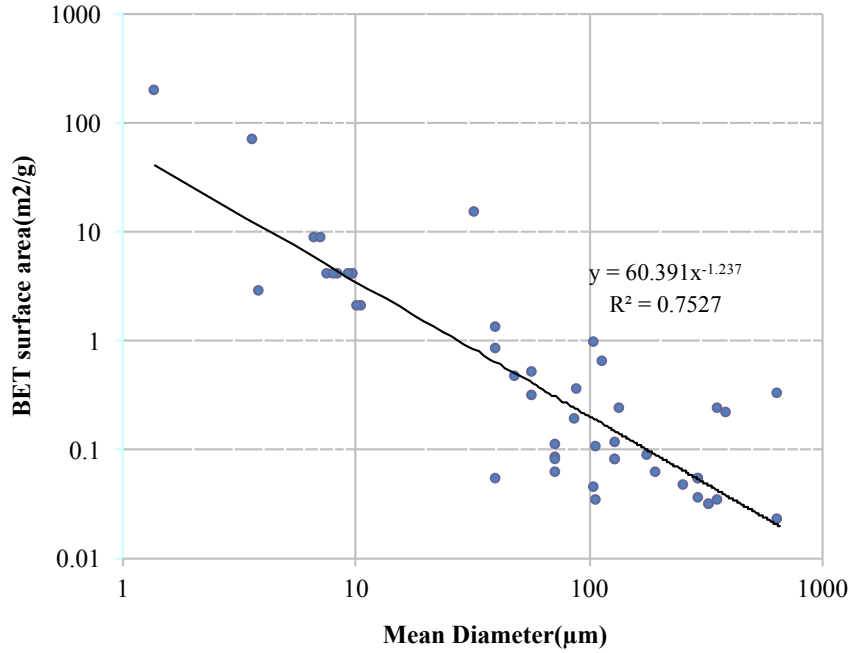


Figure 6.2: Plot of SSA ($\text{m}^2 \text{g}^{-1}$) measured by BET vs. particle diameter (μm) obtained through past studies.

Grain-type	Measured SSA (from BET)	Estimated SSA
Coarse	1.07	2.2
Fine	9.78	8.89

Table 6.3: Comparison of measured and estimated SSA ($\text{m}^2 \text{g}^{-1}$)

6.5 Calculation of thickness of the ‘surface layer’

The following section calculates the thickness of the Si-rich ‘surface layer’; using **coarse** particles as an example.

Start date of experiment = 5 June 2015

Last date of measurement = 14 March 2016

Number of days water added² = 274 days

Water added = 75 ml d^{-1}

Total water added = $274 \times 75 = 20\,550 \text{ ml} = 20.55 \text{ l}$

$\text{Mg}^{+2}_{\text{avg, coarse}}$ (between start and end date) = $590 \mu\text{mol l}^{-1}$

Total Mg^{+2} released = $620 \times 20.55 \times 10^{-6} \text{ mol} = 0.0127 \text{ mol}$

Molecular Mass of Mg = 24.3 g mol^{-1}

Total Mg^{+2} released = $0.0127 \times 24.3 = 0.31 \text{ g}$

²excluding weekends and public holidays

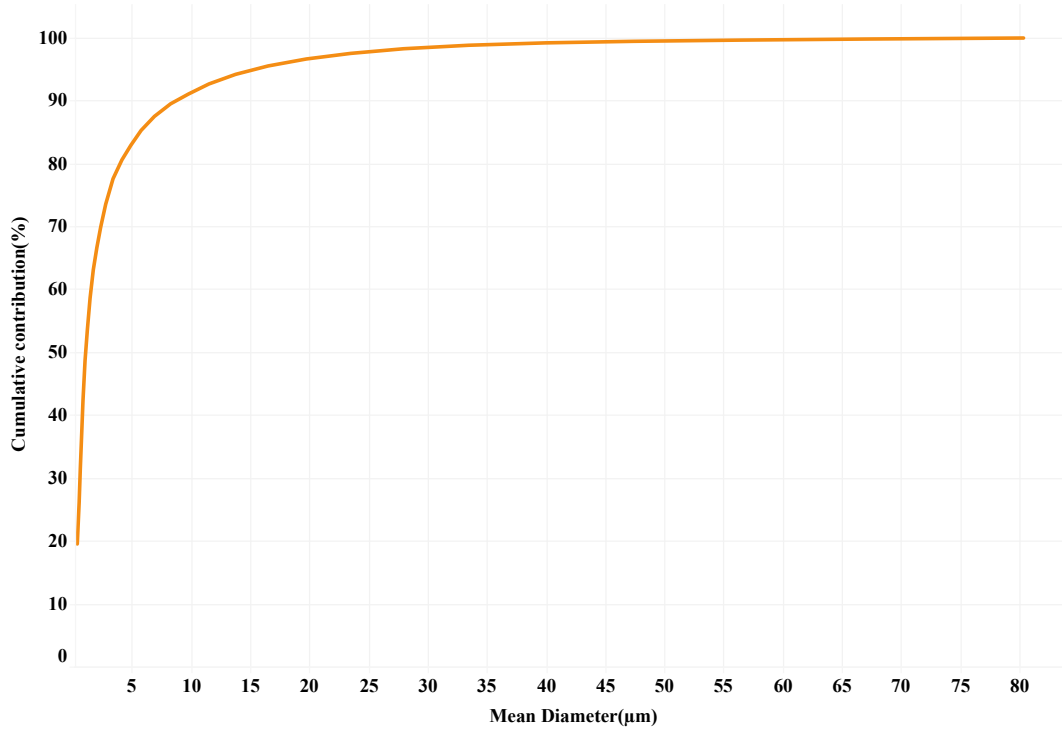


Figure 6.3: Plot of cumulative contribution of a particle with diameter D to the total of the surface areas (in percent) vs. mean particle diameter (in μm) for fine grain-type

At stoichiometry, Total $\text{Si}_{\text{released}} = \frac{0.0127}{1.88} = 0.00676 \text{ mol}$

Molecular mass of dissolved silica (H_4SiO_4) = 96.11 g mol^{-1}

Total $\text{Si}_{\text{released}} = 0.00676 \times 96.11 = 0.65 \text{ g}$

Observed $\text{Si}_{\text{avg}} = 9.8 \mu\text{mol l}^{-1}$

Total $\text{Si}_{\text{observed}} = 9.8 \times 20.55 = 201.39 \times 10^{-6} \text{ mol}$

Total $\text{Si}_{\text{observed}} = 201.39 \times 96.11 \times 10^{-6} \text{ g} = 0.019 \text{ g}$

Total $\text{Si}_{\text{precipitated}} = \text{Total Si}_{\text{released}} - \text{Total Si}_{\text{observed}}$

$\text{Si}_{\text{precipitated}} = 0.65 - 0.019 = 0.631 \text{ g}$

Assuming that all $\text{Si}_{\text{precipitated}}$ forms a uniform layer of Si around the mineral surface:

Density of Si-layer = 1.32 g cm^{-3}

Average TSA of coarse particles = 1041.95 m^2

$\text{Mass}_{\text{Si}} = \text{Density}_{\text{Si}} \times \text{Volume}_{\text{Si}}$

$\text{Volume}_{\text{Si}} = \text{Thickness}_{\text{Si}} \times \text{TSA}$

$\text{Thickness}_{\text{Si}} = \frac{\text{Mass}_{\text{Si}}}{\text{Density}_{\text{Si}} \times \text{TSA}}$

$\text{Thickness}_{\text{Si}} = \frac{0.631}{1.32 \times 1041.95} \times 10^{-4} \text{ cm} = 4.7 \times 10^{-8} \text{ cm} = 4.7 \times 10^{-10} \text{ m} = 0.47 \text{ nm}$

Mean Diameter (μm)	Weight fraction	SSA (from regression equation, $\text{m}^2 \text{g}^{-1}$)	Surface area (m^2)
80.30	0.053	0.266	0.014
67.32	0.047	0.331	0.016
56.35	0.041	0.412	0.017
47.39	0.043	0.511	0.022
39.90	0.053	0.632	0.034
33.41	0.062	0.787	0.049
27.93	0.067	0.982	0.066
23.44	0.065	1.220	0.079
19.70	0.065	1.513	0.099
16.45	0.063	1.890	0.119
13.71	0.057	2.368	0.135
11.47	0.049	2.953	0.143
9.73	0.038	3.619	0.138
8.23	0.040	4.454	0.178
6.86	0.035	5.581	0.198
5.74	0.030	6.960	0.211
4.87	0.024	8.531	0.206
4.11	0.026	10.5	0.268
3.36	0.027	13.5	0.359
2.74	0.019	17.3	0.322
2.32	0.014	21.3	0.290
2.00	0.012	25.7	0.313
1.70	0.013	31.4	0.402
1.42	0.011	39.1	0.438
1.20	0.009	48.3	0.445
1.00	0.009	60.6	0.564
0.82	0.007	76.9	0.530
0.70	0.004	94.1	0.423
0.60	0.004	113.9	0.490
0.50	0.004	142.9	0.586
0.34	0.008	229.1	1.742
			8.894

Table 6.4: Mean diameter and weight fraction from laser granulometry, SSA from regression equation, and surface area as the product of weight fraction and BET area for fine grain-type.

A similar calculation can be done for fine and mixed particles.

Mean Diameter (μm)	Weight fraction	SSA (from regression equation, m ² g ⁻¹)	Surface area (m ²)
2254.0	0.0066	0.004	0.00003
1895.5	0.0148	0.005	0.00008
1595.9	0.0325	0.007	0.00021
1336.4	0.0589	0.008	0.00048
1117.0	0.0850	0.010	0.00087
937.7	0.0973	0.013	0.00124
787.9	0.1072	0.016	0.00169
658.2	0.1060	0.020	0.00209
548.5	0.0949	0.025	0.00234
458.8	0.0774	0.031	0.00238
389.2	0.0575	0.038	0.00217
329.1	0.0556	0.046	0.00258
274.2	0.0439	0.058	0.00256
229.4	0.0330	0.073	0.00240
194.6	0.0233	0.089	0.00207
164.5	0.0214	0.110	0.00234
134.4	0.0190	0.141	0.00267
109.7	0.0111	0.181	0.00201
92.8	0.0069	0.222	0.00153
79.8	0.0055	0.268	0.00147
67.8	0.0051	0.328	0.00167
56.9	0.0043	0.408	0.00175
47.9	0.0035	0.504	0.00176
39.9	0.0037	0.632	0.00234
32.9	0.0031	0.802	0.00249
28.0	0.0023	0.981	0.00226
23.9	0.0025	1.188	0.00297
19.9	0.0026	1.491	0.00388
0.5	0.0151	142.344	2.14939
			2.20

Table 6.5: Mean diameter and weight fraction from laser granulometry, SSA from regression equation, and surface area as the product of weight fraction and BET area for coarse grain-type.

6.6 Minor ion analysis

The concentration profiles with time (Date), for the minor cations - Ca⁺², K⁺, and Na⁺ and minor anions - NO₃⁻, Cl⁻, and SO₄²⁻ are plotted in Figures 6.4 and 6.5 respectively.

	Mg_{obs} (g)	$\text{Si}_{\text{released}}$ (g)	$\text{Si}_{\text{observed}}$ (g)	Si_{ppt} (g)	Avg. TSA (m^2)	Thickness (nm)
coarse	0.31	0.65	0.019	0.63	1041.95	0.47
fine	0.75	1.58	0.018	1.56	6246.6	0.19
mixed	0.65	1.37	0.024	1.35	4771.5	0.21

Table 6.6: Results for Mg and Si released, observed, and precipitated. The Si precipitated converted to thickness of layer.

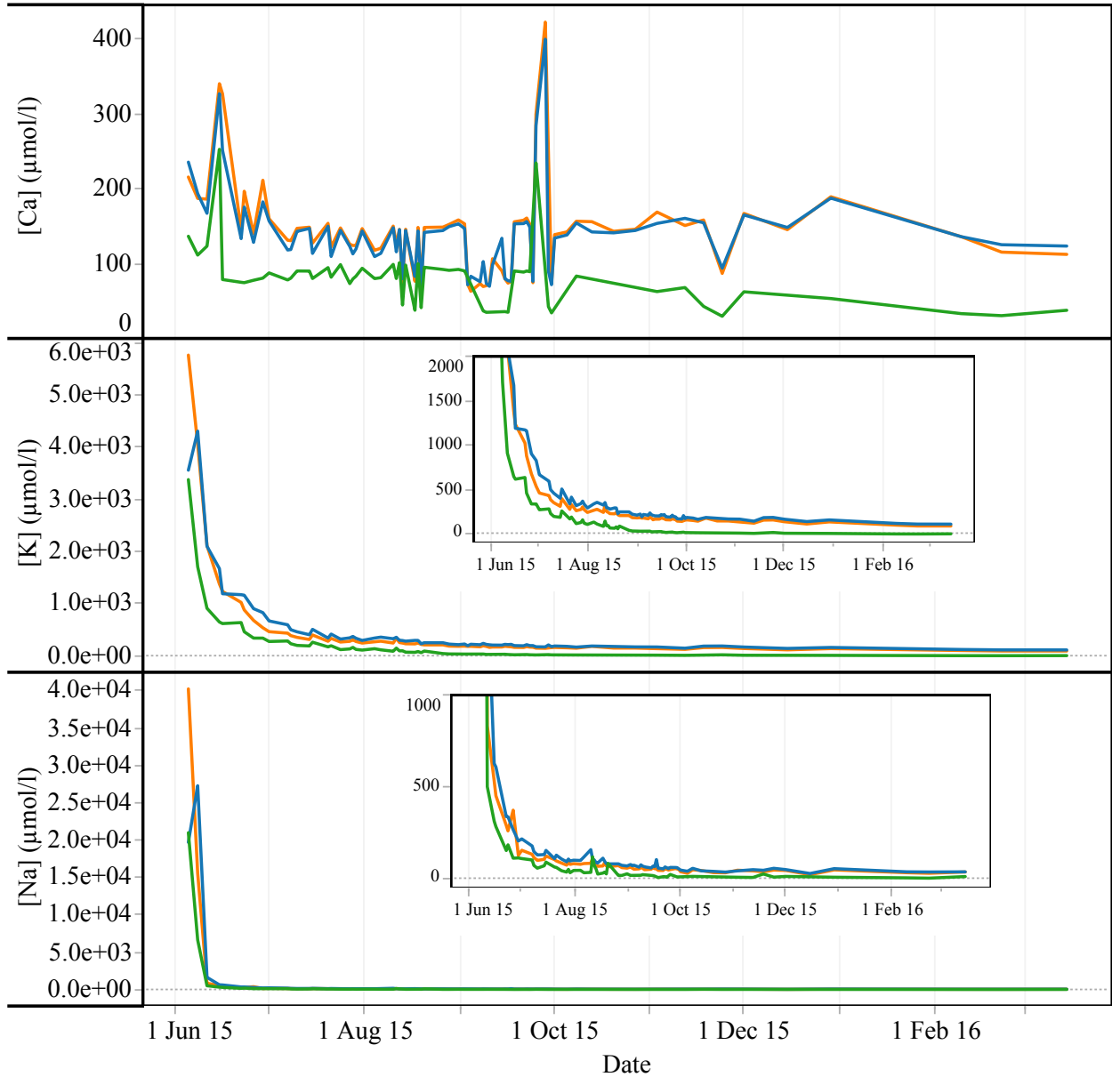


Figure 6.4: The concentration of minor ions - Ca^{+2} , K^{+} , and Na^{+} with time (Date), averaged over the three grain types - fine, coarse, and mixed.

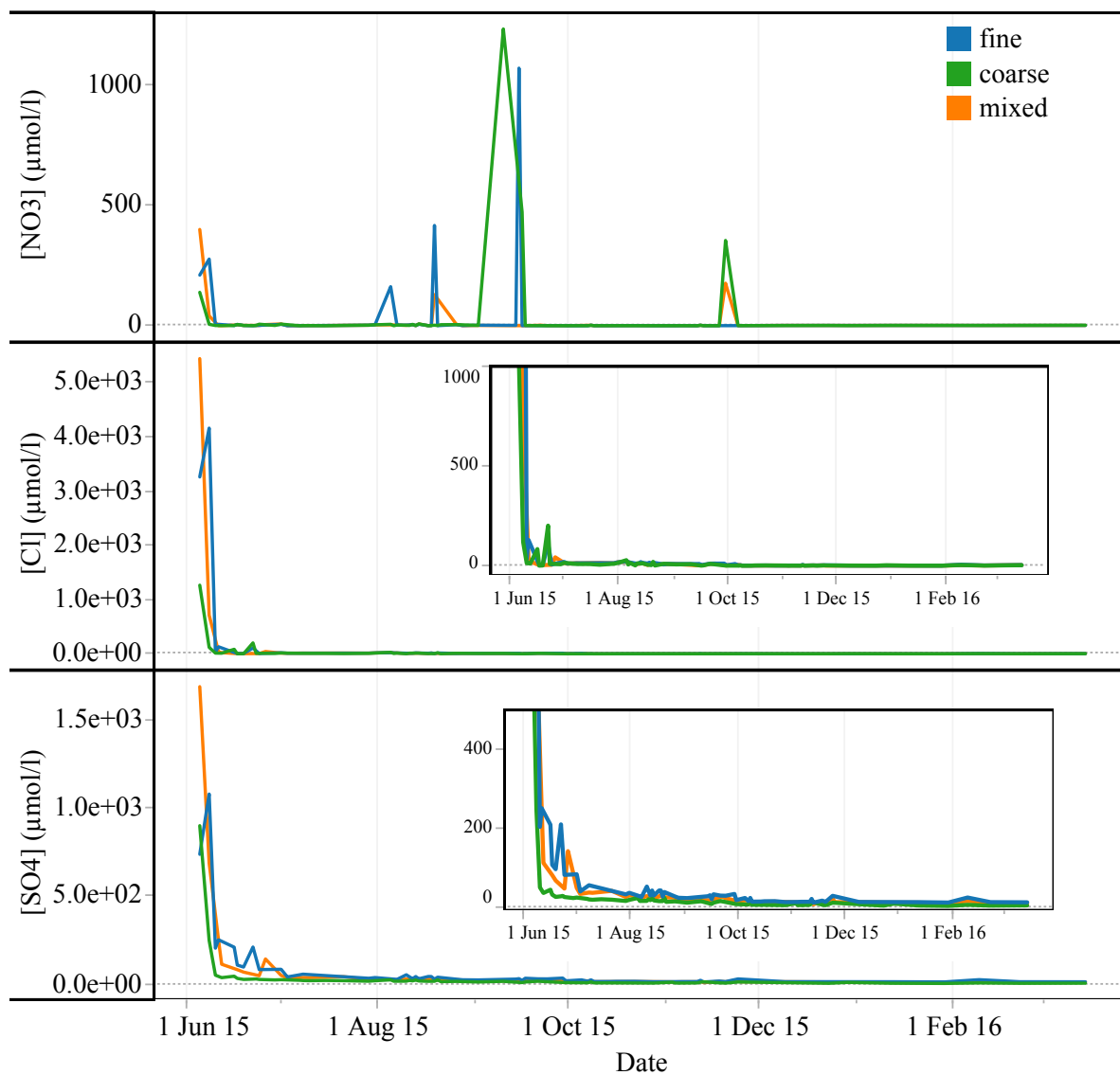


Figure 6.5: The concentration of minor ions - NO_3^- , Cl^- , and SO_4^{2-} with time (Date), averaged over the three grain types - fine, coarse, and mixed.

Bibliography

- Aagaard, P. and H. C. Helgeson (1982). Thermodynamic and kinetic constraints on reaction rates among minerals and aqueous solutions; i, theoretical considerations. *American Journal of Science* 282(3), 237–285.
- Awad, A., A. K. Van Groos, and S. Guggenheim (2000). Forsteritic olivine: effect of crystallographic direction on dissolution kinetics. *Geochimica et Cosmochimica Acta* 64(10), 1765–1772.
- Bearat, H., M. McKelvy, A. Chizmeshya, D. Gormley, R. Nunez, R. Carpenter, K. Squires, and G. Wolf (2006). Carbon sequestration via aqueous olivine mineral carbonation: role of passivating layer formation. *Environmental Science & Technology* 40(15), 4802–4808.
- Brady, P. V. and J. V. Walther (1989). Controls on silicate dissolution rates in neutral and basic pH solutions at 25°C. *Geochimica et Cosmochimica Acta* 53(11), 2823–2830.
- Brantley, L. (2008a). Kinetics of mineral dissolution. In L. Brantley, D. J. Kubicki, and F. A. White (Eds.), *Kinetics of Water-Rock Interaction*, pp. 151–210. New York, NY: Springer New York.
- Brantley, L. S. (2008b). Analysis of rates of geochemical reactions. In L. S. Brantley, D. J. Kubicki, and F. A. White (Eds.), *Kinetics of Water-Rock Interaction*, pp. 151–210. New York, NY: Springer New York.
- Brantley, S. L. and N. P. Mellott (2000). Surface area and porosity of primary silicate minerals. *American Mineralogist* 85(11-12), 1767–1783.
- Brunauer, S., P. Emmett, and E. Teller (1938). Adsorption of gases in multimolecular layers. *Journal of the American Chemical Society* 60(2), 309–319.
- Coninck, H. d., M. Loos, B. Metz, O. Davidson, and L. Meyer (2005). Ipcc special report

on carbon dioxide capture and storage. Technical report, Intergovernmental Panel on Climate Change.

Coulson, J., J. Richardson, J. Backhurst, and J. Harker (1991). *Vol. 2: Particle technology and separation processes* (5 ed.), Chapter Flow of Fluids through Granular Beds and Packed Columns, pp. 95–145. Oxford [etc.]: Butterworth-Heinemann.

Golubev, S. V., O. S. Pokrovsky, and J. Schott (2005). Experimental determination of the effect of dissolved CO_2 on the dissolution kinetics of Mg and Ca silicates at 25°C. *Chemical Geology* 217(3), 227–238.

Grandstaff, D. (1978). Changes in surface area and morphology and the mechanism of forsterite dissolution. *Geochimica et Cosmochimica Acta* 42(12), 1899–1901.

Hänchen, M., V. Prigiobbe, G. Storti, T. Seward, and M. Mazzotti (2006). Dissolution kinetics of fosteritic olivine at 90–150 °C including effects of the presence of CO_2 . *Geochimica et Cosmochimica Acta* 70(17), 4403–4416.

Hangx, S. and C. Spiers (2009). Coastal spreading of olivine to control atmospheric CO_2 concentrations: a critical analysis of viability. *International Journal of Greenhouse Gas Control* 3(6), 757–767.

Hartmann, J. and N. Moosdorf (2012). The new global lithological map database GLiM: A representation of rock properties at the Earth surface. *Geochemistry, Geophysics, Geosystems* 13(12).

Hartmann, J., A. West, P. Renforth, P. Köhler, C. De La Rocha, D. Wolf-Gladrow, H. Dürr, and J. Scheffran (2013). Enhanced chemical weathering as a geoengineering strategy to reduce atmospheric carbon dioxide, supply nutrients, and mitigate ocean acidification. *Reviews of Geophysics* 51(2), 113–149.

Helgeson, H. C., W. M. Murphy, and P. Aagaard (1984). Thermodynamic and kinetic constraints on reaction rates among minerals and aqueous solutions. ii. rate constants, effective surface area, and the hydrolysis of feldspar. *Geochimica et Cosmochimica Acta* 48(12), 2405–2432.

Hellmann, R., R. Wirth, D. Daval, J.-P. Barnes, J.-M. Penisson, D. Tisserand, T. Epicier, B. Florin, and R. L. Hervig (2012). Unifying natural and laboratory chemical weathering with interfacial dissolution–reprecipitation: a study based on the nanometer-scale chemistry of fluid–silicate interfaces. *Chemical Geology* 294, 203–216.

- Holdren, G. R. and R. A. Berner (1979). Mechanism of feldspar weathering—i. experimental studies. *Geochimica et Cosmochimica Acta* 43(8), 1161–1171.
- Holdren, G. R. and P. M. Speyer (1987). Reaction rate-surface area relationships during the early stages of weathering. ii. data on eight additional feldspars. *Geochimica et Cosmochimica Acta* 51(9), 2311–2318.
- Johnson, C. L., M. J. Hÿtch, and P. R. Buseck (2004). Displacement and strain fields around a [100] dislocation in olivine measured to sub-angstrom accuracy. *American Mineralogist* 89(10), 1374–1379.
- Keitzel, M. (2015). Mineralogische charakterisierung von sedimentproben aus einem mesokosmosexperiment mit dunit im oberboden. Master's thesis, Institute of Geology, University of Hamburg.
- Kleiv, R. and M. Thornhill (2006). Mechanical activation of olivine. *Minerals Engineering* 19(4), 340–347.
- Köhler, P., J. Hartmann, and D. A. Wolf-Gladrow (2010). Geoengineering potential of artificially enhanced silicate weathering of olivine. *Proceedings of the National Academy of Sciences* 107(47), 20228–20233.
- Lasaga, A. (1995). Fundamental approaches in describing mineral dissolution and precipitation rates. *Reviews in Mineralogy and Geochemistry* 31(1), 23–86.
- Lee, M. R., M. E. Hodson, D. J. Brown, M. MacKenzie, and C. L. Smith (2008). The composition and crystallinity of the near-surface regions of weathered alkali feldspars. *Geochimica et Cosmochimica Acta* 72(20), 4962–4975.
- Luce, R. W., R. W. Bartlett, and G. A. Parks (1972). Dissolution kinetics of magnesium silicates. *Geochimica et Cosmochimica Acta* 36(1), 35–50.
- Luttge, A. and R. S. Arvidson (2008). The mineral-water interface. In L. Brantley, D. J. Kubicki, and F. A. White (Eds.), *Kinetics of Water-Rock Interaction*, pp. 73–108. New York, NY: Springer New York.
- Manutchehr-Danai, M. (2009). *Weathering*, pp. 917–917. Berlin, Heidelberg: Springer Berlin Heidelberg.
- Martinez, R. E., S. Weber, and K. Bucher (2014). Quantifying the kinetics of olivine dissolution in partially closed and closed batch reactor systems. *Chemical Geology* 367, 1–12.

- Meybeck, M. (1987). Global chemical weathering of surficial rocks estimated from river dissolved loads. *American Journal of Science* 287(5), 401–428.
- Moosdorf, N., P. Renforth, and J. Hartmann (2014). Carbon dioxide efficiency of terrestrial enhanced weathering. *Environmental Science & Technology* 48(9), 4809–4816.
- Nimmo, J. (2004). Porosity and pore size distribution. *Encyclopedia of Soils in the Environment* 3, 295–303.
- Oelkers, E. H. (2001). An experimental study of forsterite dissolution rates as a function of temperature and aqueous mg and si concentrations. *Chemical Geology* 175(3), 485–494.
- Paces, T. (1973). Steady-state kinetics and equilibrium between ground water and granitic rock. *Geochimica et Cosmochimica Acta* 37(12), 2641–2663.
- Pokrovsky, O. and J. Schott (2000). Kinetics and mechanism of forsterite dissolution at 25c and ph from 1 to 12. *Geochimica et Cosmochimica Acta* 64(19), 3313–3325.
- Renforth, P., P. P. von Strandmann, and G. Henderson (2015). The dissolution of olivine added to soil: Implications for enhanced weathering. *Applied Geochemistry* 61, 109–118.
- Rimstidt, J. D. (2013). *Geochemical rate models: an introduction to geochemical kinetics*. Cambridge University Press.
- Rimstidt, J. D. (2015). Diffusion control of quartz and forsterite dissolution rates. *Applied Geochemistry* 61, 99–108.
- Rimstidt, J. D., S. L. Brantley, and A. A. Olsen (2012). Systematic review of forsterite dissolution rate data. *Geochimica et Cosmochimica Acta* 99, 159–178.
- Rosso, J. J. and J. D. Rimstidt (2000). A high resolution study of forsterite dissolution rates. *Geochimica et Cosmochimica Acta* 64(5), 797–811.
- Schott, J. and R. A. Berner (1985). Dissolution mechanisms of pyroxenes and olivines during weathering. In *The chemistry of weathering*, pp. 35–53. Springer.
- Schott, J., R. A. Berner, and E. L. Sjöberg (1981). Mechanism of pyroxene and amphibole weathering—i. experimental studies of iron-free minerals. *Geochimica et Cosmochimica Acta* 45(11), 2123–2135.

- Schott, J., O. S. Pokrovsky, and E. H. Oelkers (2009). The link between mineral dissolution/precipitation kinetics and solution chemistry. *Reviews in Mineralogy and Geochemistry* 70(1), 207–258.
- Schuiling, R. and P. Krijgsman (2006). Enhanced weathering: An effective and cheap tool to sequester CO_2 . *Climatic Change* 74(1-3), 349–354.
- Shepherd, J. (2009). *Geoengineering the climate: science, governance and uncertainty*. Royal Society.
- Tester, J. W., W. G. Worley, B. A. Robinson, C. O. Grigsby, and J. L. Feerer (1994). Correlating quartz dissolution kinetics in pure water from 25°C to 625°C. *Geochimica et Cosmochimica Acta* 58(11), 2407–2420.
- Tilley, C. E. and W. B. Simmons (2016). Olivine.
- Tobiesen, A. E. D. (2016). Classification of olivin (0-3 mm) with respect to marpol annex v criteria. Technical report, Norwegian institute for water research.
- White, A. (2002). An integrated approach for determining mineral weathering rates based on regolith solute and solute elemental gradients: application to biotite weathering in saprolites. *Chemical Geology* 190, 69–89.
- White, A. F. and S. L. Brantley (1995). Chemical weathering rates of silicate minerals: an overview. *Chemical Weathering Rates of Silicate Minerals* 31, 1–22.
- White, A. F. and S. L. Brantley (2003). The effect of time on the weathering of silicate minerals: why do weathering rates differ in the laboratory and field? *Chemical Geology* 202(3), 479–506.
- White, A. F. and M. L. Peterson (1990). Role of reactive-surface-area characterization in geochemical kinetic models. In *ACS symposium series*, Volume 416, pp. 461–475. Oxford University Press.
- Wogelius, R. and J. Walther (1991). Olivine dissolution at 25°C: Effects of pH, CO_2 , and organic acids. *Geochimica et Cosmochimica Acta* 55(4), 943–954.
- Wogelius, R. and J. Walther (1992). Olivine dissolution kinetics at near-surface conditions. *Chemical Geology* 97(1-2), 101–112.
- Zou, R., M. Gan, and A. Yu (2011). Prediction of the porosity of multi-component mixtures of cohesive and non-cohesive particles. *Chemical Engineering Science* 66(20), 4711–4721.

Acknowledgments

I'm thankful to the following people:

To, Tom Jaepinnen and Peggy Barsch for being extremely kind and caring colleagues in the laboratory. Working with them was fun and I learned much from them; especially from the mistakes which they covered for me.

To my friends, Barbara Hof, Lukas Stein, Felix Schreyer, and Julius Garbe who took interest in my stories of olivine and 'rate control'. They provided me with valuable ideas and suggestions for my thesis. Their friendship and companionship during this time is highly valued.

To my supervisor, Prof. Jens Hartmann who offered me his full support during my time at his working group and when I temporarily left it mid-way to work in Berlin. I thank him for having trust in me and providing me with many opportunities; things every young researcher needs.

To my second supervisor, Dr. Thorben Amann, who was 'unlucky' in having his office right opposite to mine! I constantly troubled him with questions and doubts, but he patiently and whole-heartedly engaged in discussions.

To the Stein's 'down south': Silke, Klaus, Damaris, and Valentin; who provided me with the love and warmth of home and family.

To my own family in India: Aakriti, Achal, Geeta, and Pulkit Malik; for motivating me and supporting my decisions.

Lastly, I'm thankful to myself, for persisting, pushing, and finding a way ahead. Taking decisions was difficult but I believed in myself.

Declaration of Academic Integrity

“Hiermit versichere ich an Eides statt, dass ich die vorliegende Arbeit im Studiengang School of Integrated Climate System Science) selbstständig verfasst und keine anderen als die angegebenen Hilfsmittel – insbesondere keine im Quellenverzeichnis nicht benannten Internet-Quellen – benutzt habe. Alle Stellen, die wörtlich oder sinngemäß aus Veröffentlichungen entnommen wurden, sind als solche kenntlich gemacht. Ich versichere weiterhin, dass ich die Arbeit vorher nicht in einem anderen Prüfungsverfahren eingereicht habe und die eingereichte schriftliche Fassung der auf dem elektronischen Speichermedium entspricht.”

Place, Date, Name Signature